CHAPTER 5

RESULT AND DISCUSSION

5.1 Results of raw material characterization

5.1.1 Chemical composition

Table 5.1 Chemical analysis of raw materials by XRF compared with Hypure Vector®.

Chemical analysis	BCW	K325	B85	VECTOR*
%SiO_2	54.10	44.80	44.30	**49.45%**
%Al_2O_3	27.20	37.70	38.20	**32.29%**
%Fe_2O_3	1.88	0.81	0.58	**1.31%**
%TiO_2	0.22	0.03	0.03	**1.01%**
%CaO	0.31	0.07	0.09	**0.30%**
%MgO	0.33	0.06	0.08	**0.50%**
%K_2O	2.20	1.09	0.85	**2.22%**
%Na_2O	0.34	0.14	0.01	**0.30%**
%LOI	13.60	14.10	14.60	**12.61%**
%P_2O_5	0.02	<0.01	<0.01	
%MnO	<0.01	0.02	0.02	
%Cr_2O_3	<0.01	<0.01	<0.01	

* Chemical analysis of Hypure Vector® is from ECC International Ltd.

5.1.2 Mineral composition

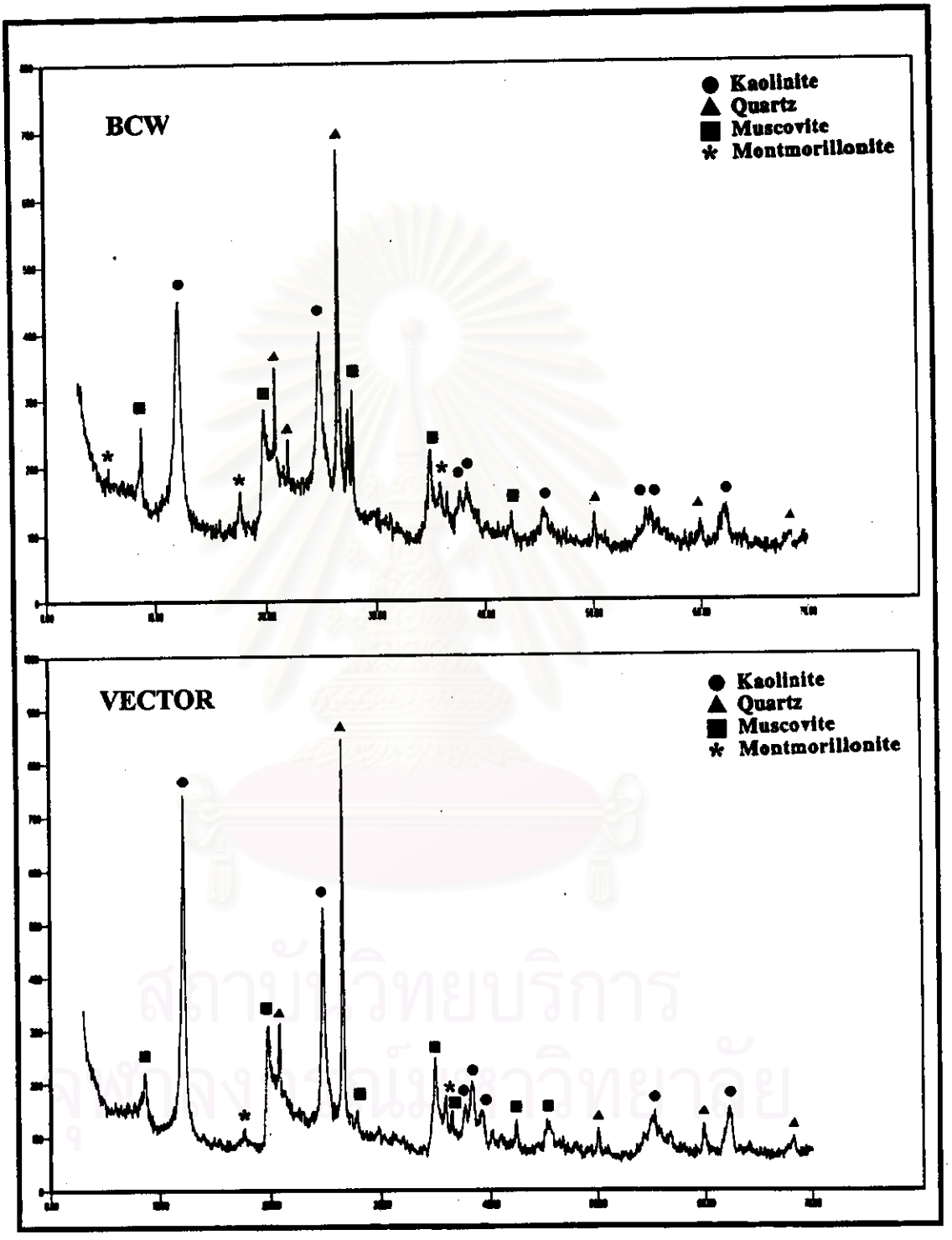

Fig 5.1 XRD patterns of BCW and Hypure Vector®.

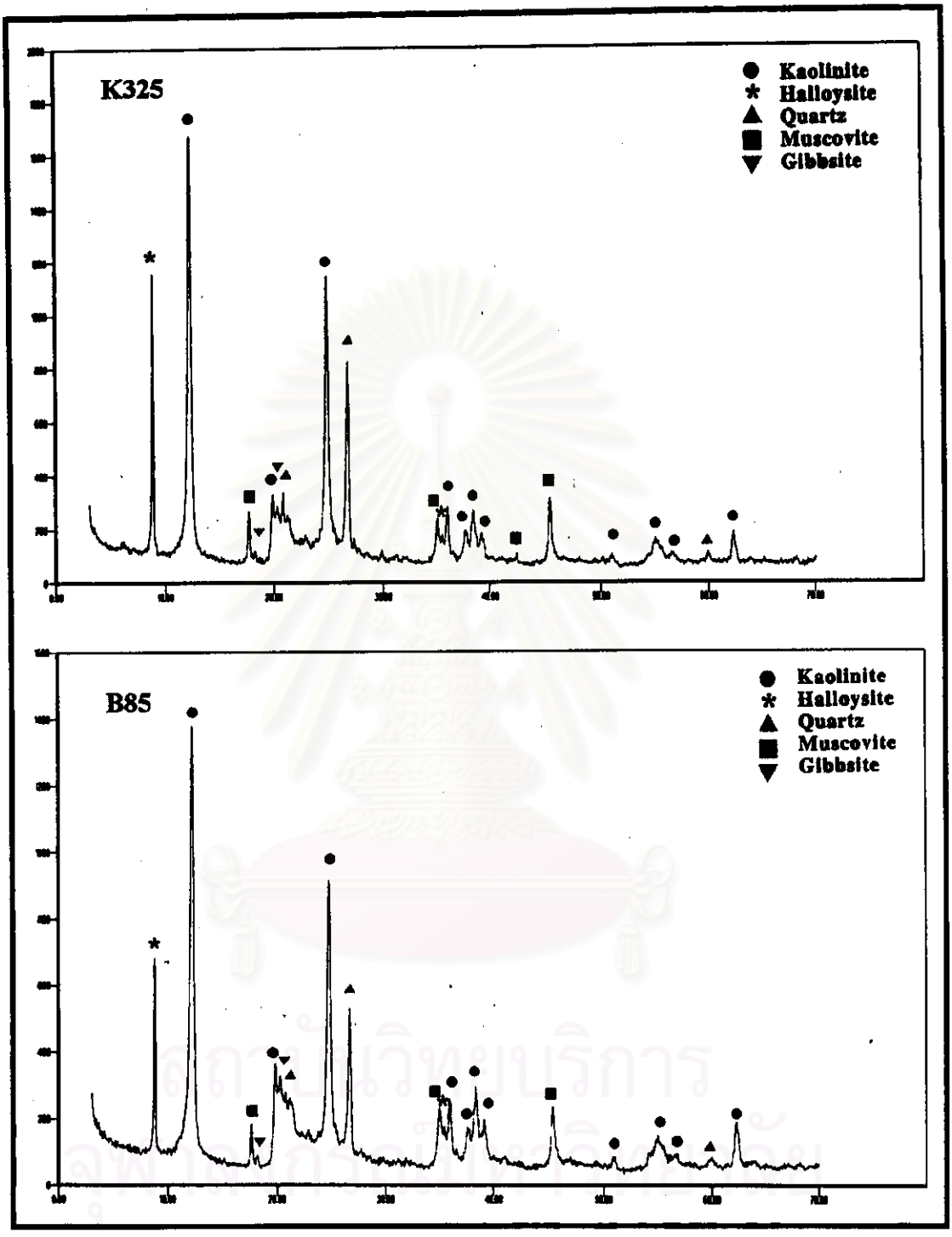

Fig 5.2 XRD patterns of K325 and B85.

Table 5.2 Mineral compositions of raw materials by XRD compared with Hypure Vector®.

Raw Materials	BCW	K325	B85	VECTOR
MINERAL	Kaolinite	Kaolinite	Kaolinite	Kaolinite
	Quartz	Halloysite	Halloysite	Quartz
	Muscovite	Muscovite	Muscovite	Muscovite
	Mont-morillonite	Quartz	Quartz	Mont-morillonite
		Gibbsite	Gibbsite	

From the chemical composition results, Table 5.1, BCW has the highest SiO_2 and the least Al_2O_3 contents when compared with those of other raw materials. BCW also has more impurities, both Fe_2O_3 and TiO_2 because it is a secondary clay which was formed by naturally chemical process known as hydrothermal alteration, washed by natural action of river or stream and deposited in sedimentary lenses. Impurities, such as the organic matters, could contaminate during alteration and sedimentation whereas K325 and B85 have less impurities because of the different deposit way. B85 contains highest content of Al_2O_3 and less impurities than K325, hence it has white color and high refractoriness after firing. B85 also has the highest loss of ignition and is followed by K325, BCW and Hypure Vector® respectively. B85 is a well crystallized kaolinite from Ranong source so the finding is contrary to the theory that LOI of ball clay should be higher. However it has long been known that Ranong clay contains some gibbsite ($Al(OH)_3$) and halloysite ($(OH)_4Al_2(Si_2O_5)2H_2O$) in the fine fraction in addition to kaolinite[25].

Mineral composition of all the employed raw materials, in general, seems to be the same composition but a little bit difference in the minor phases. The main minerals are kaolinite, quartz and muscovite. Compared with BCW and Hypure Vector®, B85 and K325 have higher kaolinite and lower quartz contents which are indicated by their high Al_2O_3 and low SiO_2 values. (Diffraction data and JCPDS data are in Appendix B)

Like B85, K325 is from Ranong source and it also has high % LOI which is contrary to its low plasticity. The term LOI covers the loss of organic matter, adsorbed moisture, metal hydroxides, carbonates, sulfides, lattice water and etc. after firing at 1000°C. Therefore, in the case of B85 and K325, the lattice water of gibbsite and halloysite is added to that of kaolinite hence results in the high %LOI. On the contrary the high %LOI of ball clays is originated from the organic matter, picked up during the course of transportation and sedimentation, which contributes to their high plasticity.

5.1.3 Thermal analysis

From DTA curve, Fig. 5.3, Hypure Vector® has two exothermic peaks at 320°C and 363°C that indicate the combustion of organic matter or carbonaceous matter. Other peaks are the endothermic peak of mineral composition and hydroxyl elimination at 527°C and the last exothermic peak of mullite recrystallisation at 976°C. All the peaks confirm the character of a kaolinite clay. From Fig. 5.4, BCW has two small endothermic peaks at 80°C and 155°C and a large exothermic peak at 374°C that indicate the presence of adsorbed moisture and the combustion of organic matter. The other peaks are the endothermic peak

of mineral composition elimination and dehydroxylation at 490°C and the last exothermic peak of mullite recrystallisation at 967°C. It can be concluded that BCW and Hypure Vector® are kaolinite clays with high organic matter. From Fig. 5.5, B85 displays a large endothermic peak from 80°C up to 250°C caused by the evolution of adsorbed water and the interlayer water, the next endothermic peak at 270°C which is due to the decomposed lattice water of typical hydrated oxides, i.e. gibbsite ($Al(OH)_3$) or goethite ($FeO(OH)$). The rest are the outstanding endothermic dehydroxylation peak at 524°C and the mullite recrystallization exothermic peak at 996°C. B85 is the well crystallized kaolinite clay compared with Hypure Vector® and BCW. B85 has no organic decomposition peak which indicate that the loss of ignition should be come from water in the lattice of gibbsite and halloysite.

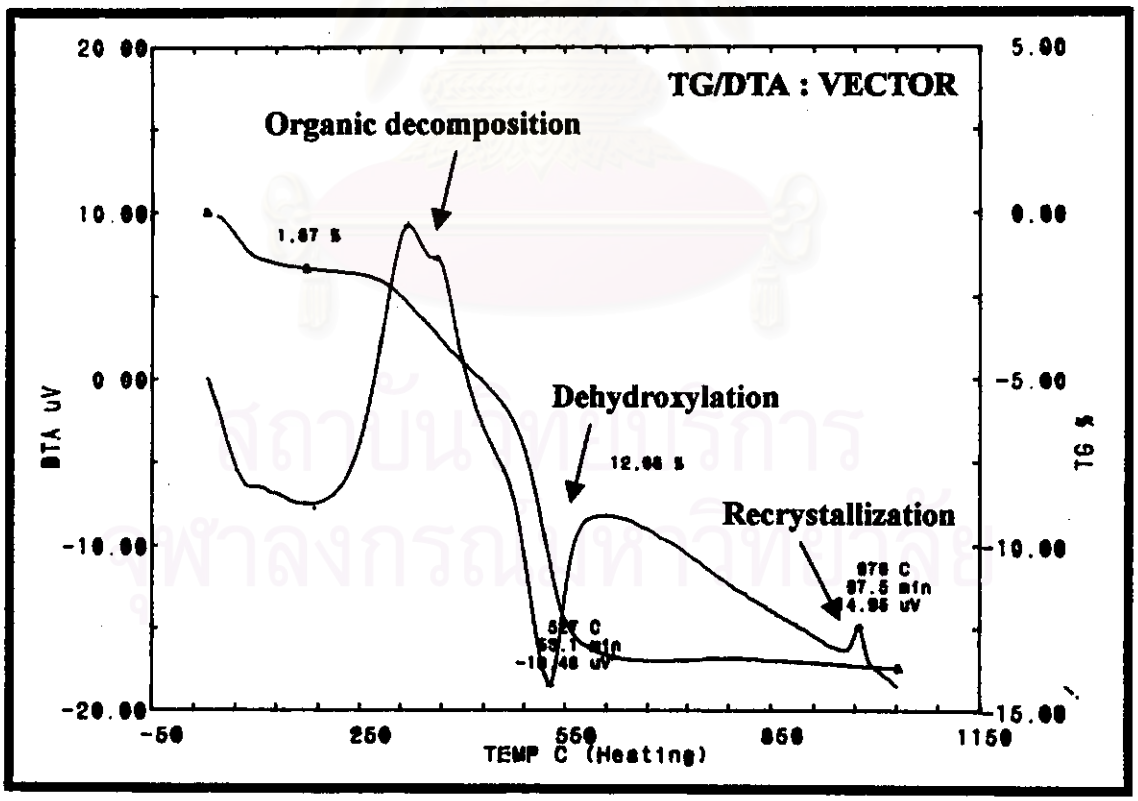

Fig 5.3 TG/DTA curves of Hypure Vector®.

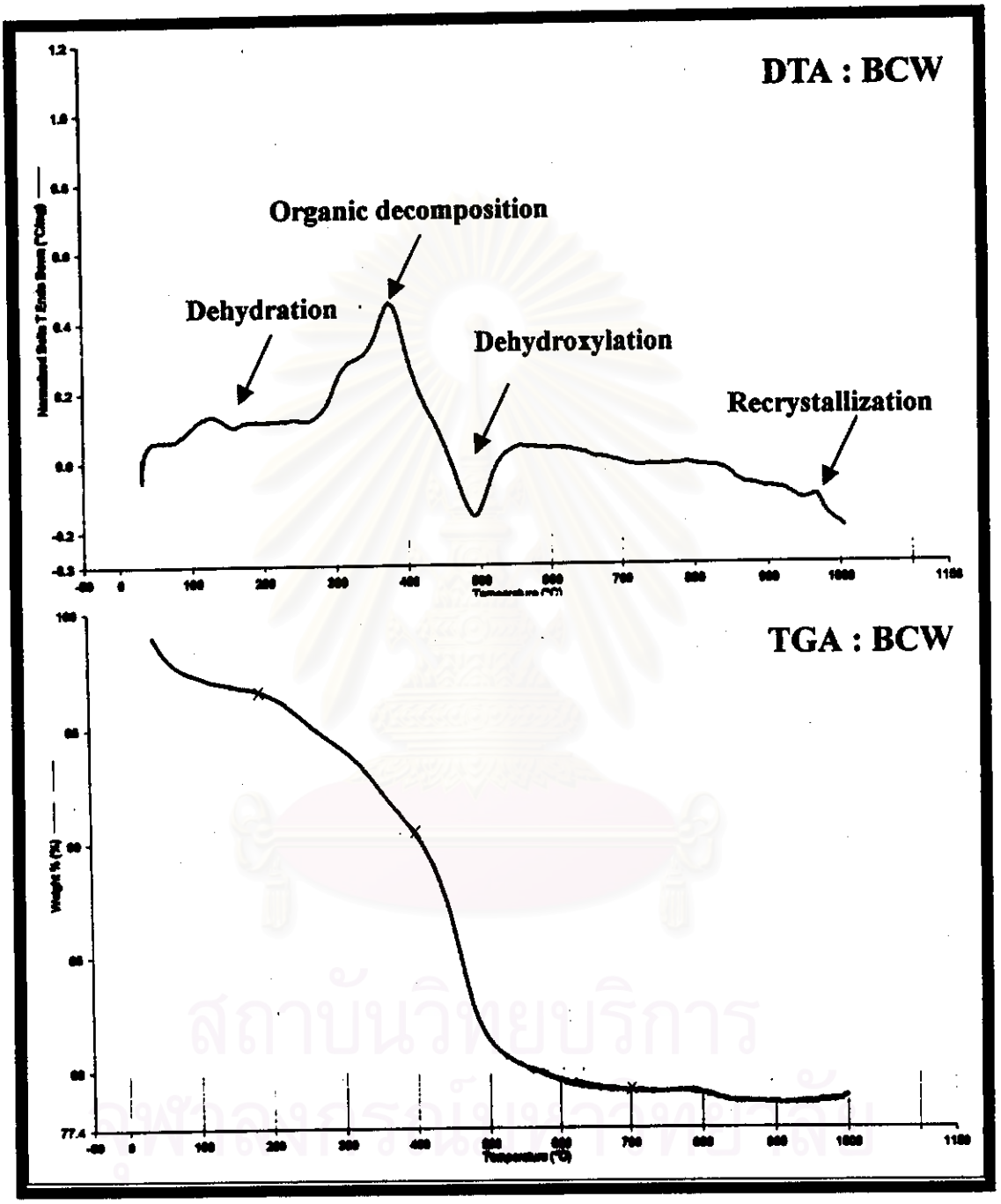

Fig 5.4 DTA and TGA curves of BCW.

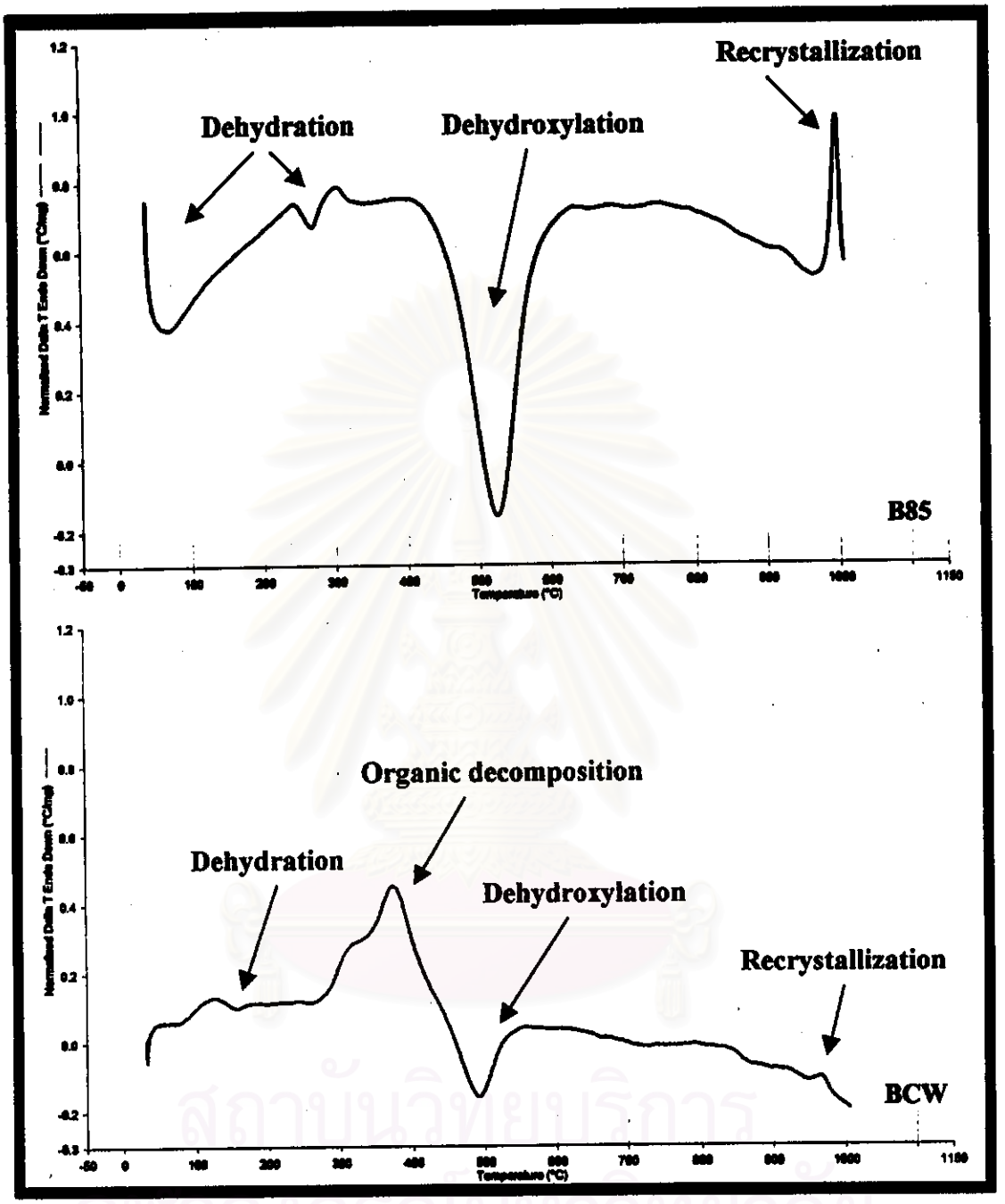

Fig 5.5 DTA curves of B85 and BCW .

5.1.4 Particle size distribution

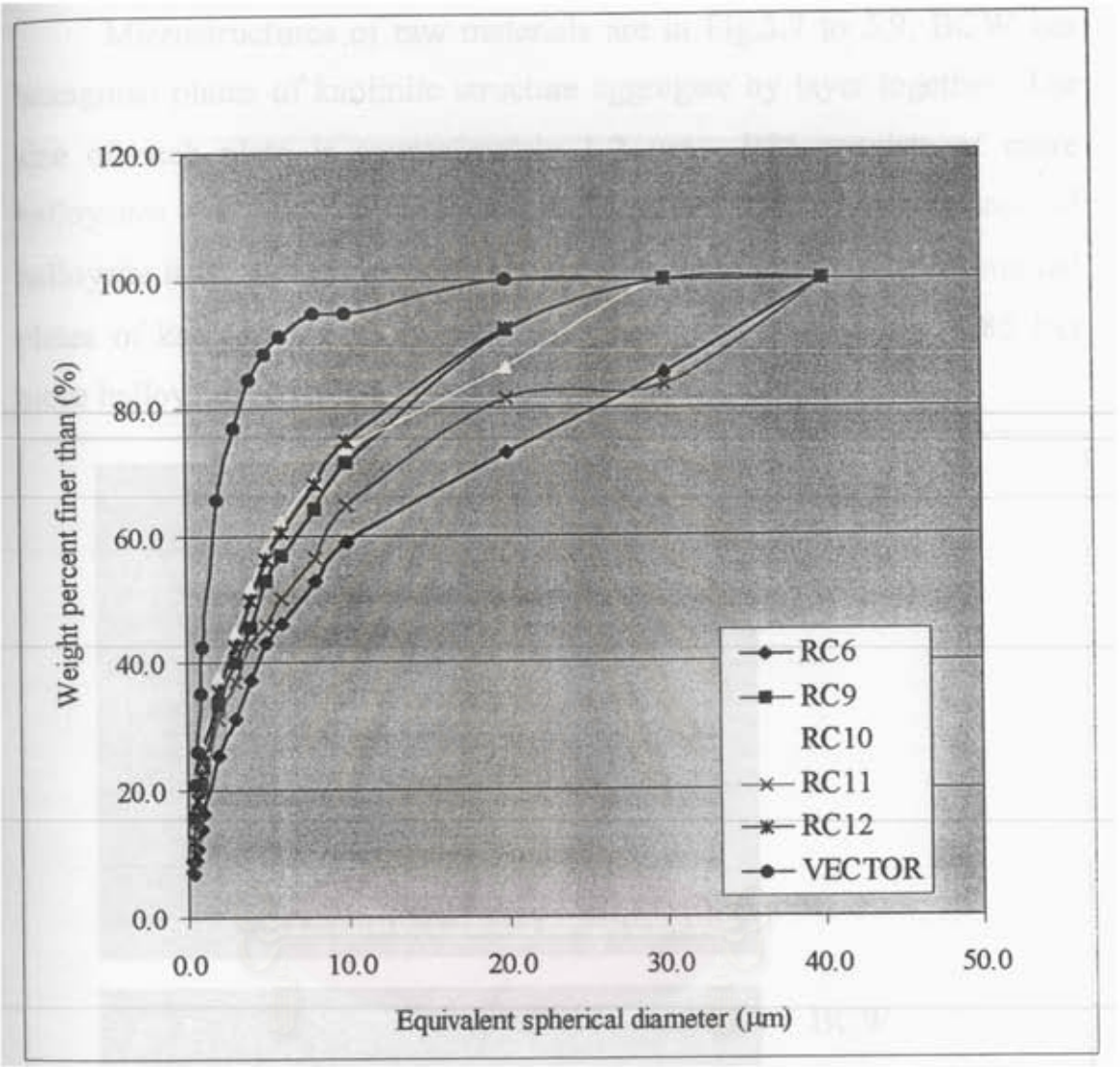

Fig. 5.6 Particle size distribution of raw materials.

BCW is the finest clay followed by Hypure Vector®, K325 and B85 in the decreasing order. The average mean particle size of BCW is 1μm. while those of Hypure Vector®, K325 and B85 are 1-2 μm., 5-6 μm. and 6-8 μm. respectively. The quantity of colloidal particles, less than 1 μm., of K325 and B85 are about four times less than BCW. It can be implied that plasticity of BCW is much higher than the two kaolins and so is the deflocculant demand.

5.1.5 Microstructure by SEM

Microstructures of raw materials are in Fig.5.7 to 5.9, BCW has hexagonal plates of kaolinite structure aggregate by layer together. The size of each plate is approximately 1-2 μm. B85 consists of more halloysites and less kaolinites compared with K325. The rod shape of halloysite is 0.2-0.4 μm in diameter and 2-6 μm in length. The hexagonal plates of kaolinite structure are 0.2-1 μm aggregate together. B85 has more halloysites so it is a little bit coarser than K325.

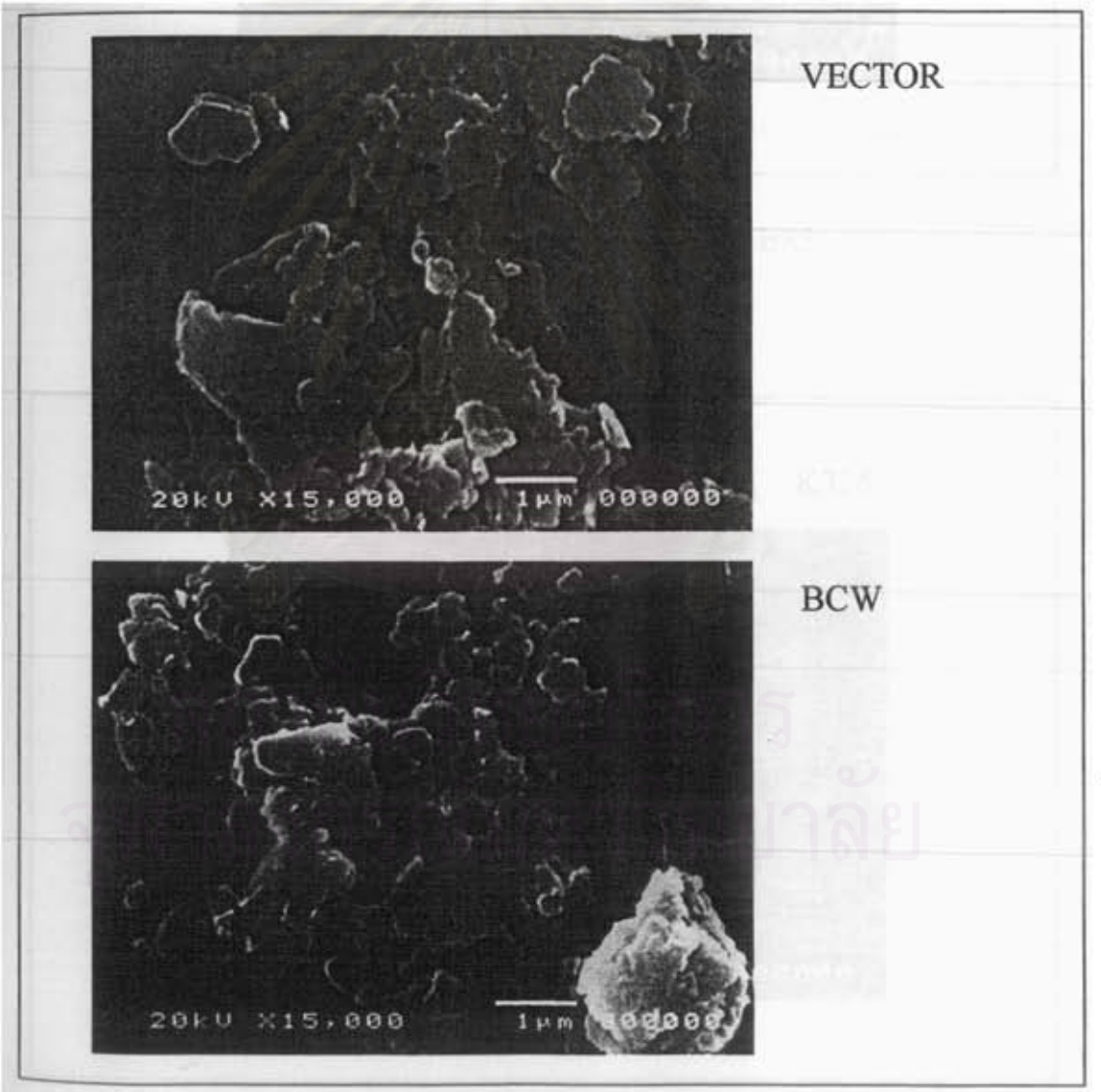

Fig 5.7 SEM micrographs of Hypure Vector® and BCW.

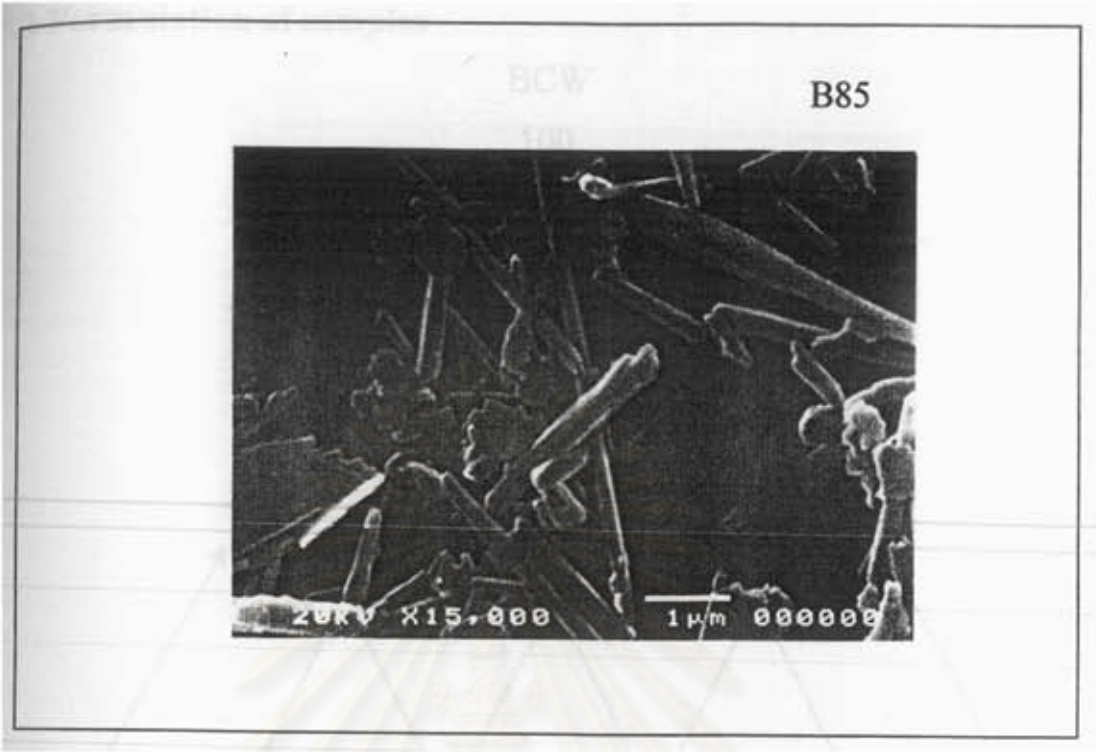

Fig 5.8 SEM micrograph of B85.

Fig 5.9 SEM micrograph of K325.

5.2 Formulation of samples

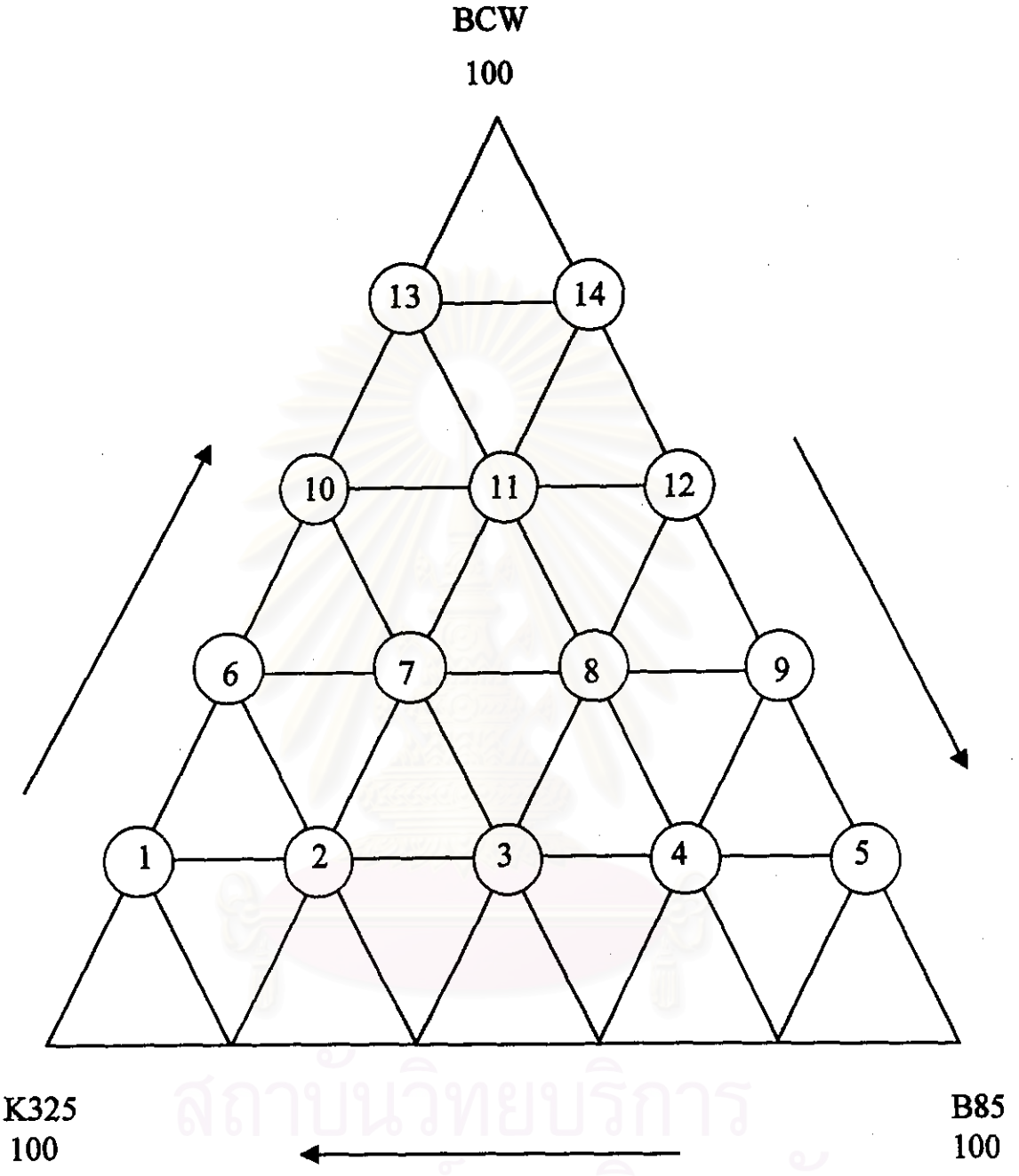

Fig 5.10 Triaxial of refined clay formulas (RC Series).

Table 5.3 RC Formulas and chemical composition by calculation.

Formula	RC 1	RC 2	RC 3	RC 4	RC 5	RC 6	RC 7	RC 8	RC 9	RC 10	RC 11	RC 12	RC 13	RC 14	VEC-TOR
BCW:K325:B85	2:8:0	2:6:2	2:4:4	2:2:6	2:0:8	4:6:0	4:4:2	4:2:4	4:0:6	6:4:0	6:2:2	6:0:4	8:2:0	8:0:2	-
% SiO_2	47.08	46.98	46.88	46.79	46.69	48.81	48.71	48.62	48.52	50.54	50.44	50.35	52.27	52.18	**49.45**
%Al_2O_3	35.96	36.06	36.17	36.27	36.38	33.76	33.86	33.97	34.07	31.55	31.66	31.77	29.35	29.46	**32.29**
%Fe_2O_3	1.03	0.98	0.94	0.89	0.85	1.24	1.20	1.15	1.10	1.45	1.41	1.36	1.67	1.62	**1.31**
%TiO_2	0.07	0.07	0.07	0.07	0.07	0.11	0.11	0.11	0.11	0.14	0.14	0.14	0.18	0.18	**1.01**
%CaO	0.12	0.12	0.13	0.13	0.13	0.17	0.17	0.17	0.18	0.21	0.22	0.22	0.26	0.27	**0.30**
%MgO	0.11	0.12	0.12	0.13	0.13	0.17	0.17	0.18	0.18	0.2	0.23	0.23	0.28	0.28	**0.50**
%K_2O	1.32	1.27	1.22	1.18	1.13	1.54	1.49	1.44	1.39	1.76	1.71	1.66	1.98	1.93	**2.22**
%Na_2O	0.18	0.15	0.13	0.10	0.08	0.22	0.19	0.17	0.14	0.26	0.23	0.21	0.30	0.27	**0.30**
%Ign.loss	14.13	14.24	14.34	14.44	14.54	13.99	14.10	14.20	14.30	13.85	13.96	14.06	13.71	13.82	**12.61**

The results of oxide composition calculated following the triaxial diagram (Fig. 5.10) is presented in Table 5.3, RC1-RC5 and RC13-14 have SiO_2 and Al_2O_3 contents different from Hypure Vector® more than 2%. RC1-RC5 have high percentage of kaolin (80% kaolin), Al_2O_3 content is higher than Hypure Vector® (3.67-4.09%), and %SiO_2 is also lower (2.37-2.76%) so they are out of the limit. RC13 and RC14 are also the same since they have high percentage of ball clay. In the range of RC6-RC9, all impurities are lower than Hypure Vector® and main oxides are in the limit, especially RC10-RC12 have higher Fe_2O_3 but lower amount of TiO_2 compared with Hypure Vector®. RC10-RC12 have the total impurities lower than Hypure Vector® so they should not give any effect on the properties after firing. RC6-RC9 should have lower deflocculant demand, whiter color after firing and less plasticity than RC10-RC12, according to their high water content (in kaolinite structure) and low organic matter.

In the range of RC6-RC9, only RC6 and RC9 are chosen to be the representative together with RC10 to RC12 because RC6 and RC9 present the properties in the minimum and maximum values of the formula proportion (60% kaolin and 40% ball clay) while RC10 and RC12 in the proportion of 40% kaolin and 60% ball clay. RC11 is the representative of formula that is composed of all three raw materials.

5.2.1 Deflocculation curves of samples at 50 wt% solid

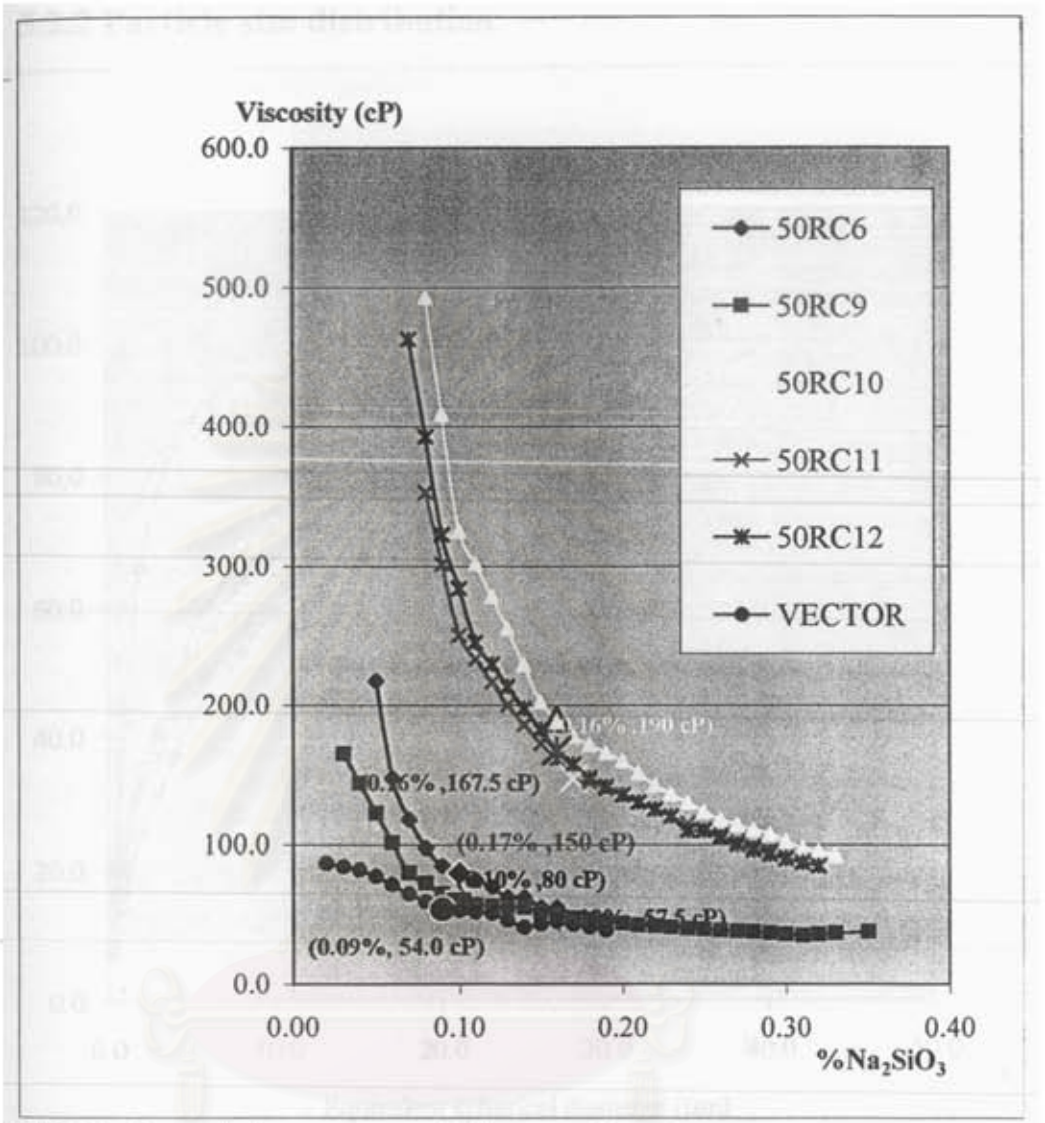

Fig 5.11 Deflocculation curves of slips at 50 wt% solid compared with Hypure Vector®.

From Fig. 5.11 (Table 1D in Appendix D), the deflocculation curves of slips can be separated in two groups. One is RC slips with 60% ball clay that have higher viscosity than the other group that have 40% ball clay and the slip property of RC9 is closer to Hypure Vector® than the other formulas. The contents of Na_2SiO_3 for fully dispersed slips of RC formulas with 60% ball clay are 0.16-0.17 wt% (based on dry weight of clay) and 0.10 wt% for RC6 and RC9 at 50 wt% solid.

5.2.2 Particle size distribution

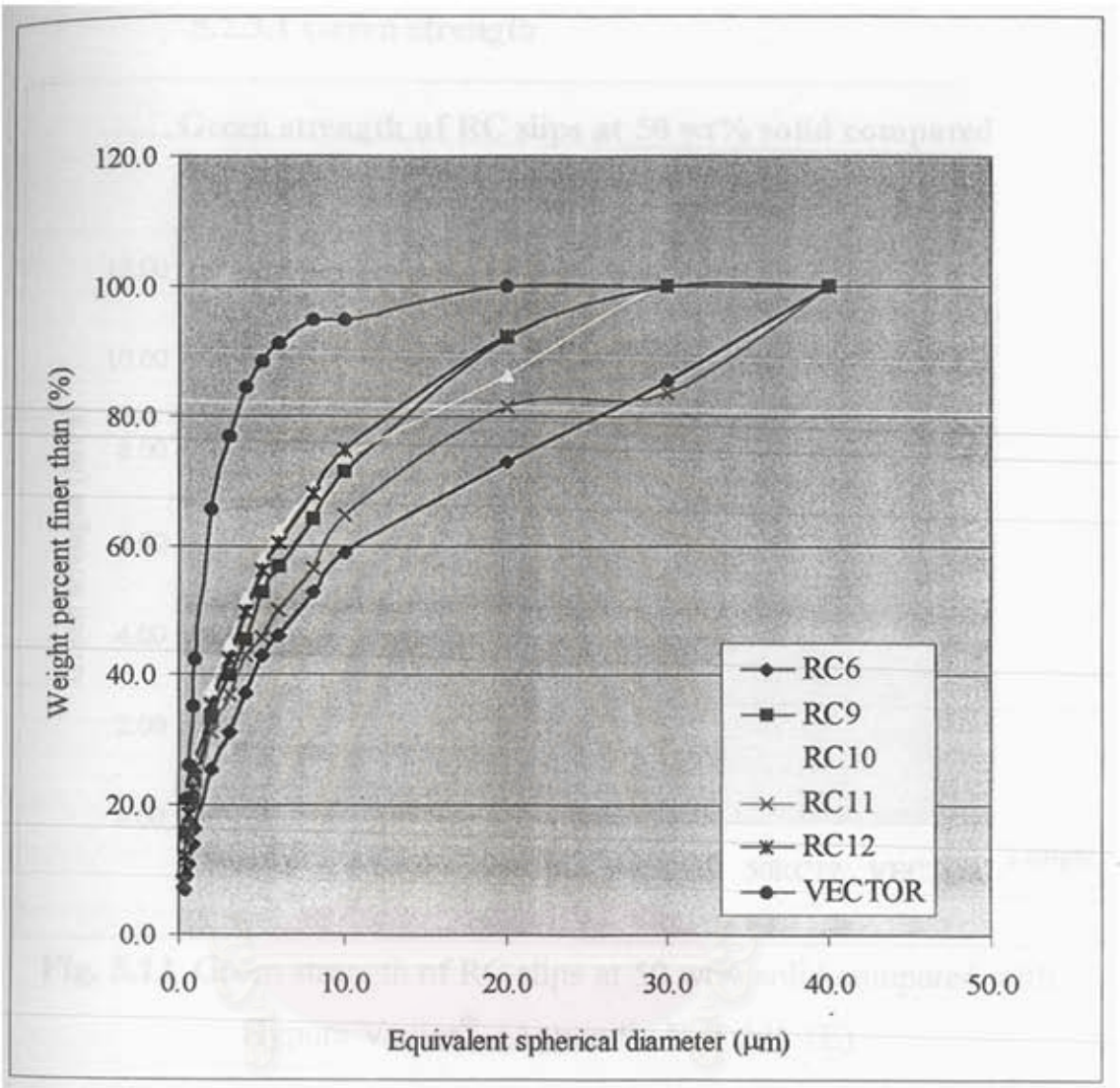

Fig 5.12 Particle size distribution of selected RC formula.

RC6 and RC9 have an average mean particle size equivalent to 6-8 μm. and 4-5 μm. while RC10, RC11 and RC12 trend to have finer average mean size equivalent to 3-4 μm., 6 μm. and 4 μm., respectively. RC6 and RC9 have the content of colloidal size (<1 μm.) is less than that of RC10-RC12 series, resulting in less plasticity and less deflocculation demand when preparing the slip corresponding with deflocculant response in Fig. 5.11 (PSD data in Appendix C-Table 3C)

5.2.3 Physical properties

5.2.3.1 Green strength

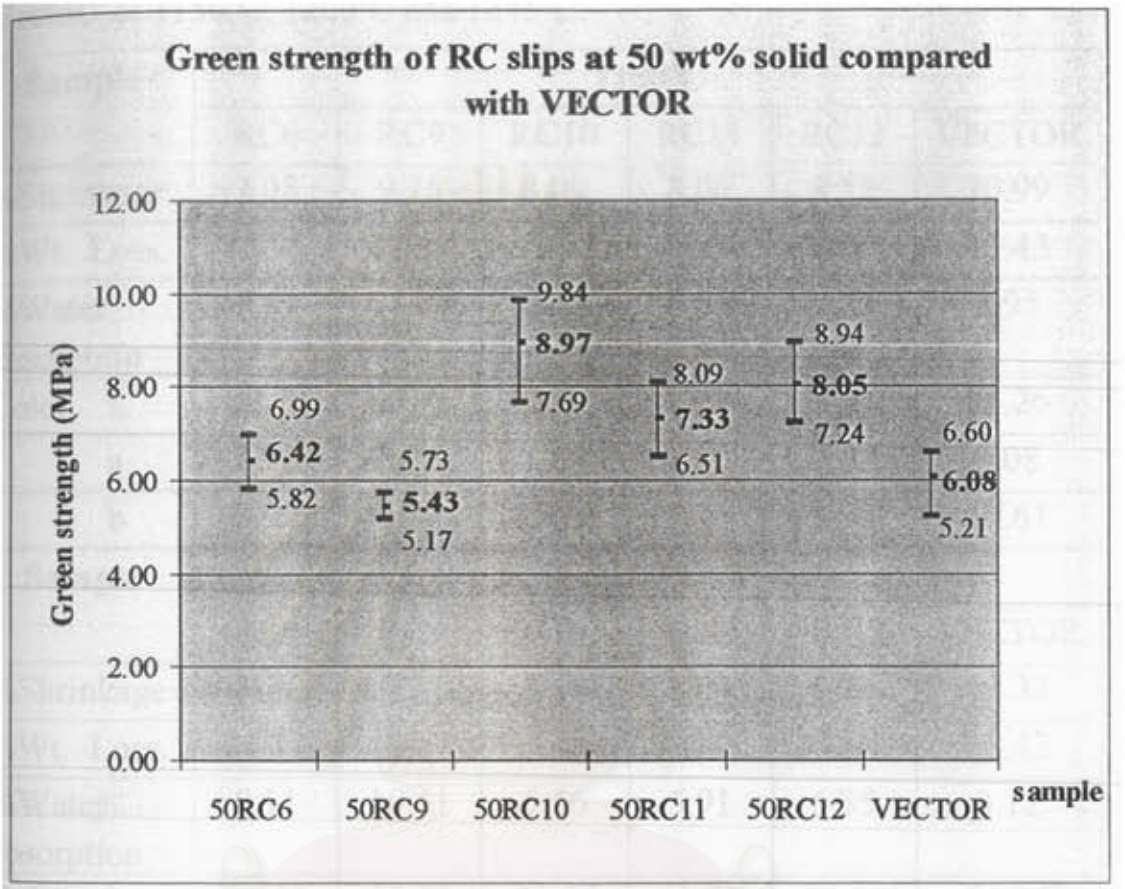

Fig. 5.13 Green strength of RC slips at 50 wt% solid compared with Hypure Vector®. (Appendix E, Table 1E)

The highest green strength is from RC10 formula, 8.97 MPa (91.46 kg/cm^2), 1.5 times higher than Hypure Vector®. Whereas RC9 has the lowest green strength this because the less ball clay content relates to less plasticity (less green strength). To discuss about the result of K325 and B85 in green strength property, K325 offers higher green strength than B85 expressed following the results of RC6 and RC10. RC11 is the only formula that consists of 3 components but the green strength is the lowest compared with RC10 and RC12. The result maybe comes from its coarser particle size distribution compared to RC10 and RC12.

5.2.3.2 Fired Properties

Table 5.4 Fired properties of samples compared with Hypure Vector® at 1150°C, 1200°C and 1245°C.

Sample	1150°C					
	RC6	RC9	RC10	RC11	RC12	VECTOR
%Shrinkage	7.08	9.26	8.09	8.60	8.55	10.99
%Wt. Loss.	11.75	12.58	11.62	11.64	11.84	13.43
%Water absorption	9.59	11.85	6.63	6.89	7.82	1.95
Color L	89.72	92.71	88.54	89.98	91.59	85.26
a	1.98	0.75	1.89	1.33	0.02	0.08
b	8.92	6.83	11.19	9.94	8.95	12.61
Sample	**1200°C**					
	RC6	RC9	RC10	RC11	RC12	VECTOR
%Shrinkage	8.77	9.27	8.64	8.64	9.20	12.33
%Wt. Loss.	11.71	12.67	11.56	11.75	11.91	13.42
%Water absorption	8.11	10.51	5.56	5.91	6.35	0.12
Color L	90.59	93.51	89.06	90.78	92.05	81.55
a	0.91	0.20	0.82	0.47	0.04	-0.15
b	8.93	6.46	11.34	10.15	9.31	13.42
Sample	**1245°C**					
	RC6	RC9	RC10	RC11	RC12	VECTOR
%Shrinkage	9.17	10.16	8.89	9.14	10.45	12.05
%Wt. Loss.	11.94	12.74	11.68	11.88	12.20	13.58
%Water absorption	6.85	8.62	4.35	4.68	5.34	0.00
Color L	91.21	94.00	90.10	91.14	92.36	79.99
a	-0.22	-0.38	-0.27	-0.31	-0.47	-0.30
b	10.80	7.11	12.83	11.59	10.51	13.29

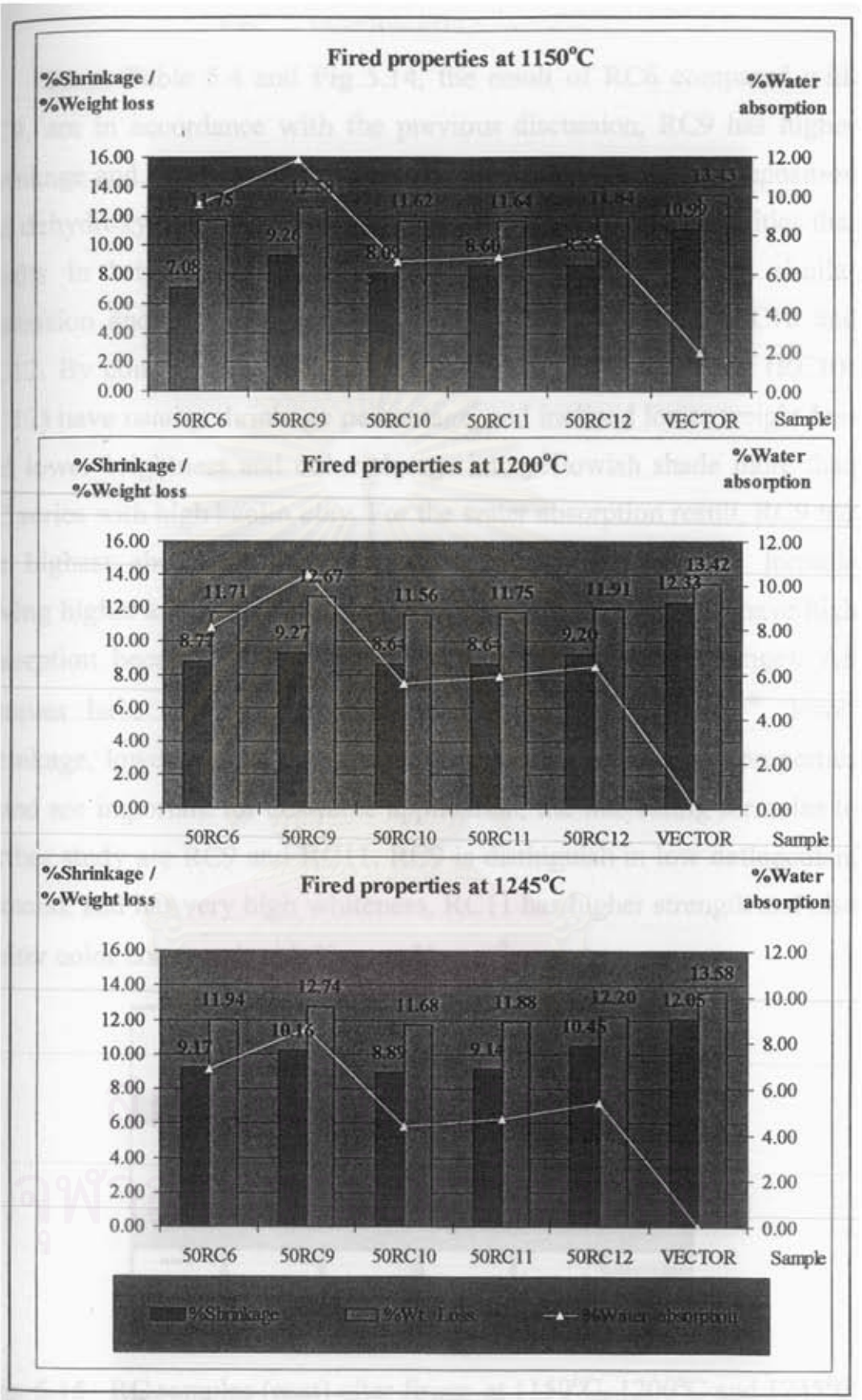

Fig. 5.14 Fired properties of samples compared with Hypure Vector®

From Table 5.4 and Fig 5.14, the result of RC6 compared with RC9, are in accordance with the previous discussion, RC9 has higher shrinkage and higher loss of ignition in the form of water decomposition and dehydroxylation. B85 has low contamination of oxide impurities that results in brighter firing color. RC10 and RC12 have the similar discussion and RC11 has the moderate properties between RC10 and RC12. By comparison, RC series with higher ball clay content (RC10-RC12) have nearby shrinkage percentage, and inclined lower weight loss and lower brightness and color change into yellowish shade more than RC series with high kaolin clay. For the water absorption result, RC9 has the highest absorption compared with other formulas. The formula having higher kaolin clay (high percentage of Al_2O_3) trends to have high absorption because of its high refractoriness (long firing range). All samples have whiter color compared with Hypure Vector®, lower shrinkage, lower weight loss and higher absorption. Since all properties found are important for desirable application, the interesting formulas to further study are RC9 and RC11. RC9 is distinguish in low deflocculant demand, and has very high whiteness, RC11 has higher strength and also whiter color compared with Hypure Vector®.

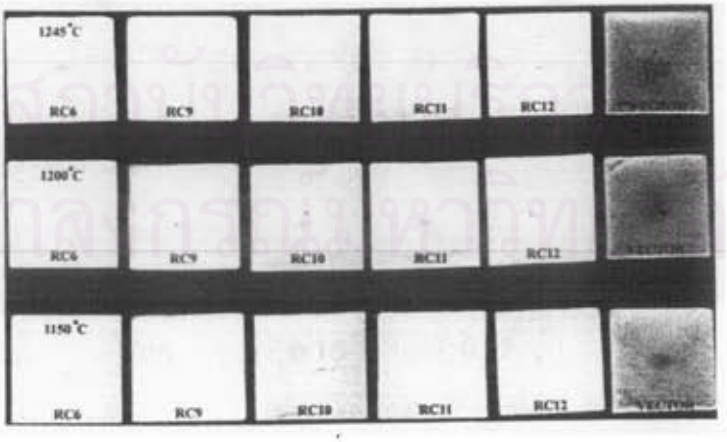

Fig. 5.15 RC samples (cast) after firing at 1150°C, 1200°C and 1245°C compared with Hypure Vector®.

5.3 Slip Characterization

5.3.1 Deflocculation curve

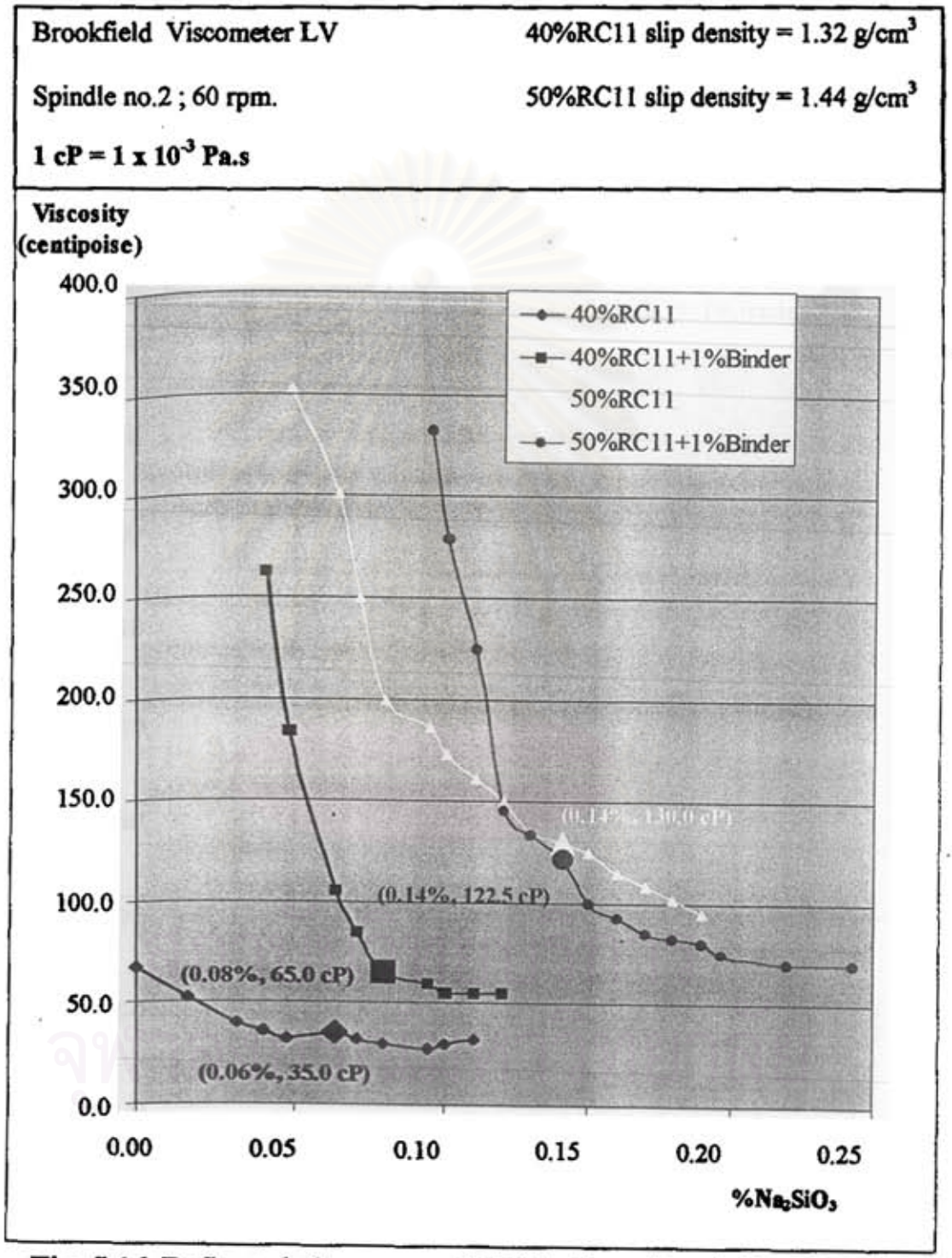

Fig. 5.16 Deflocculation curve of RC11 slip at 40 and 50 wt% solid with and without binder addition.

Brookfield Viscometer LV

50%RC9 slip density = 1.44 g/cm^3

Spindle no.2 ; 60 rpm.

1 cP = 1 x 10^{-3} Pa.s

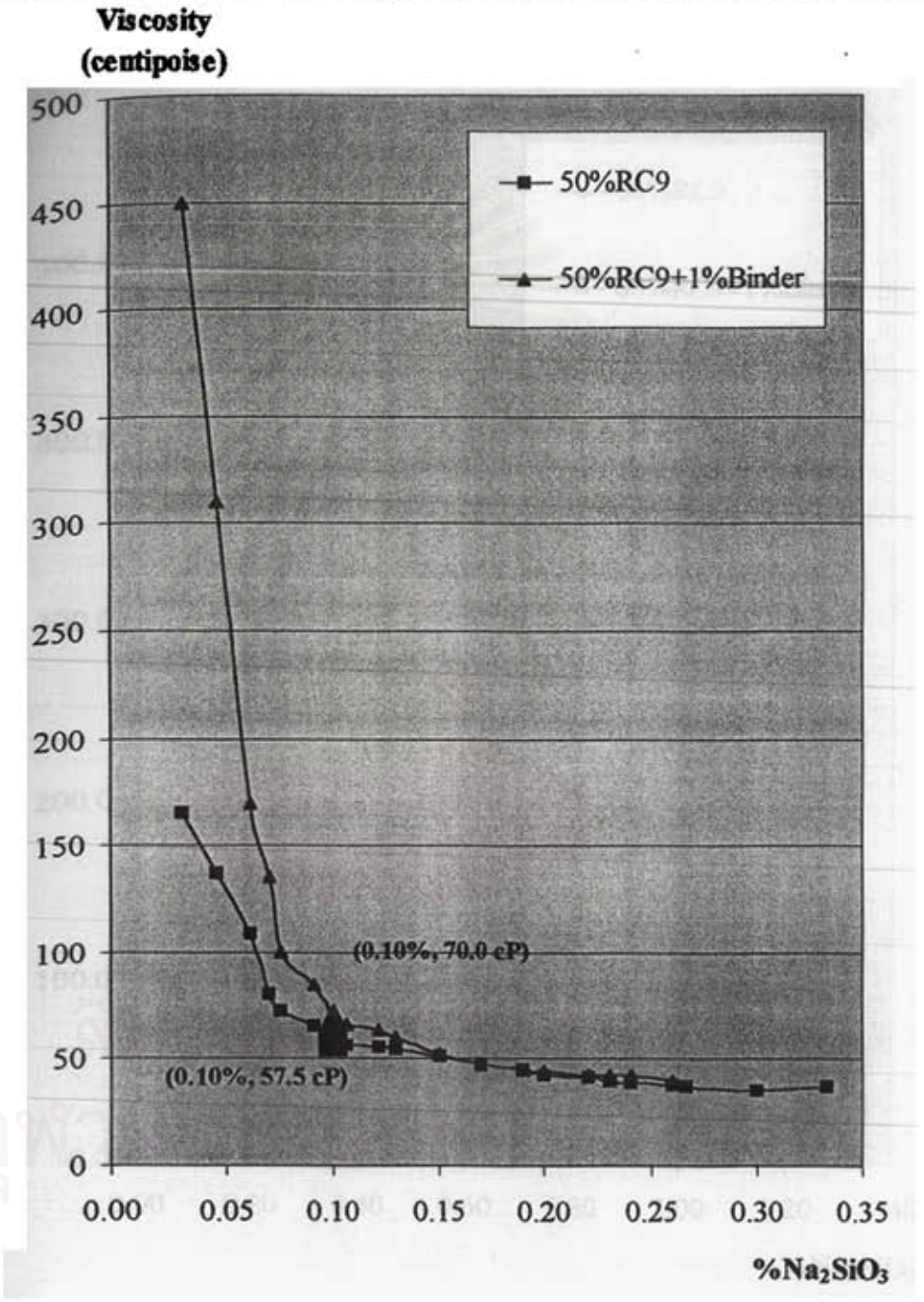

Fig. 5.17 Deflocculation curve of RC9 slip at 50 wt% solid with and without binder addition.

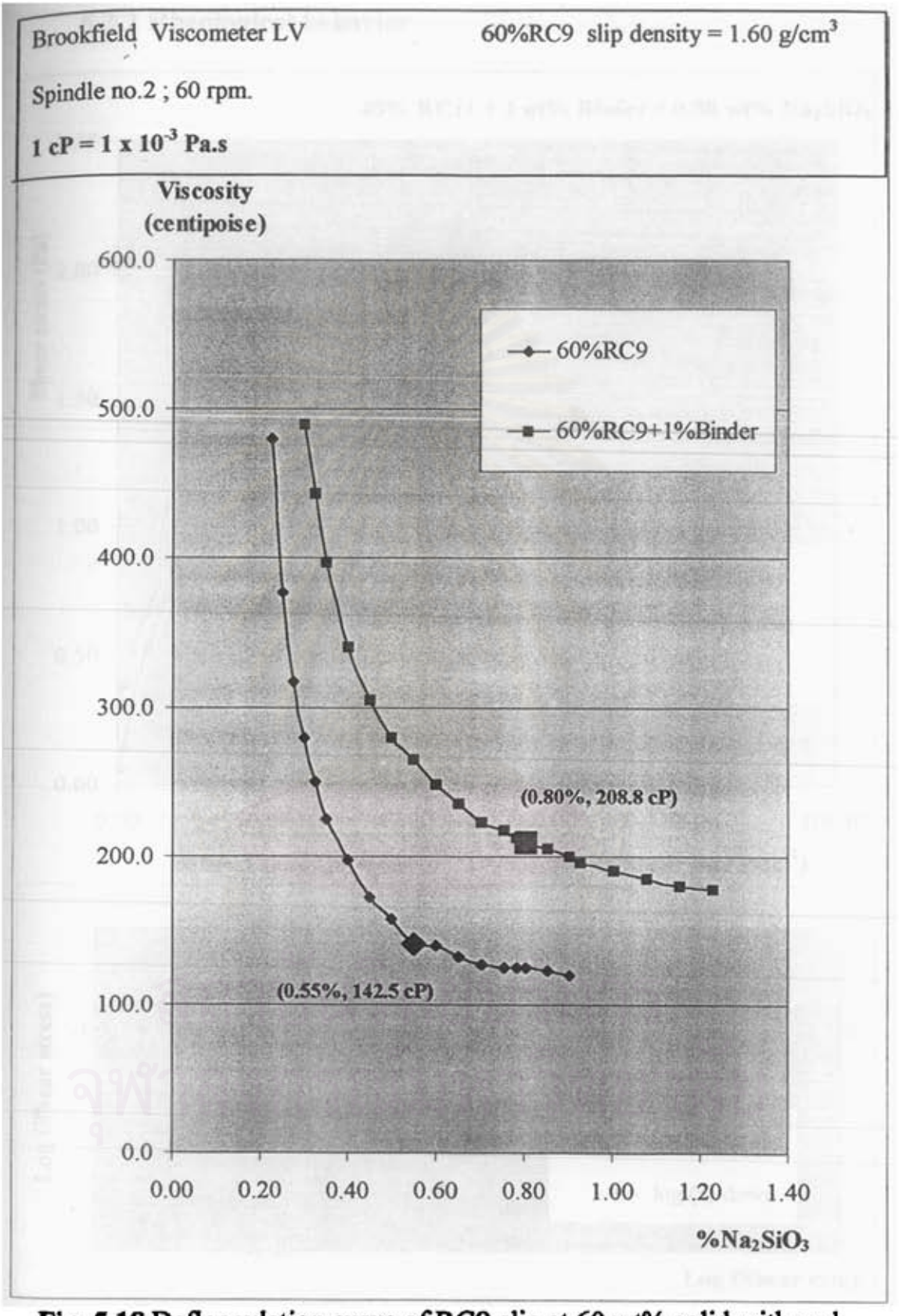

Fig. 5.18 Deflocculation curve of RC9 slip at 60 wt% solid with and without binder addition.

5.3.2 Rheological behavior

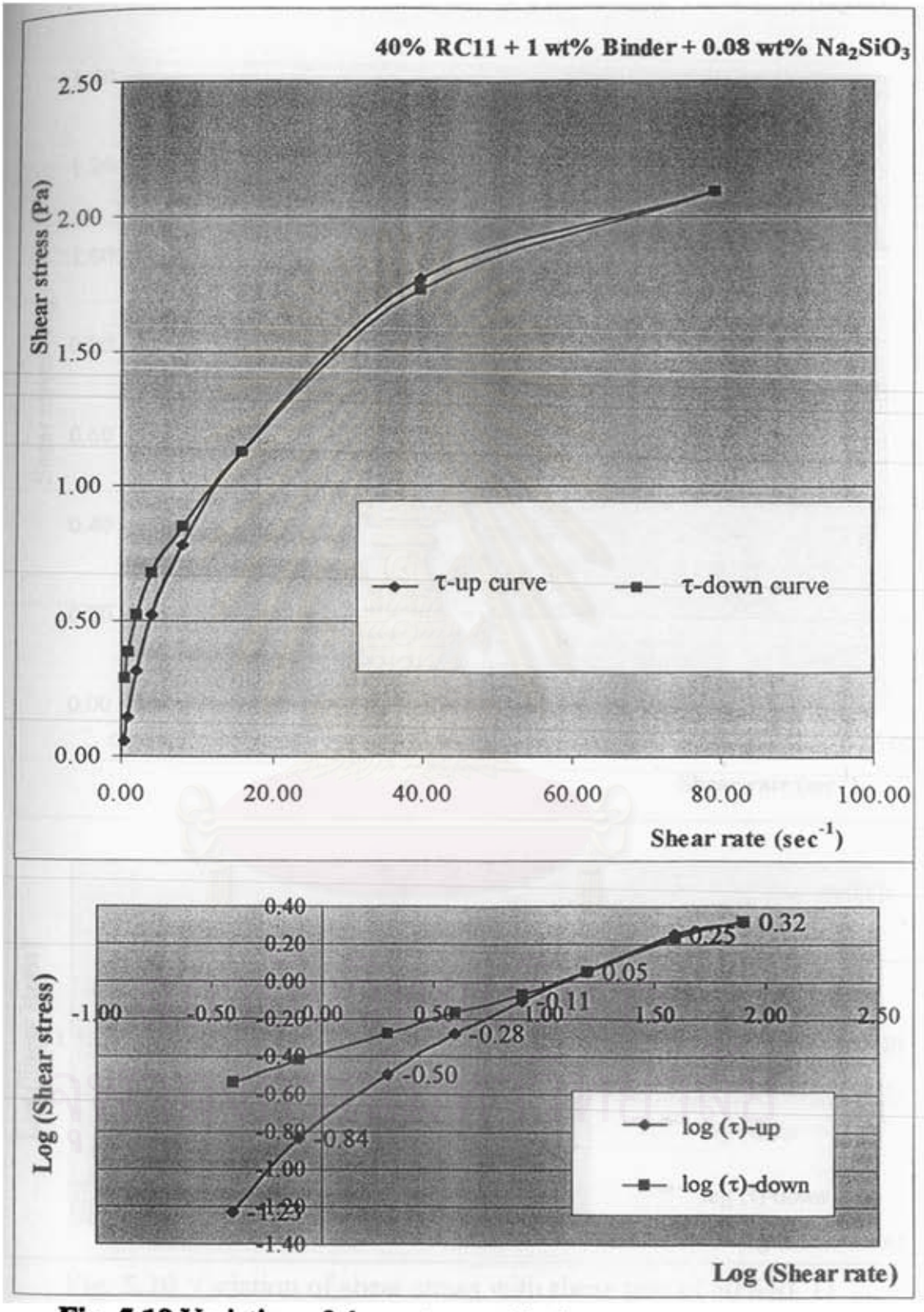

Fig. 5.19 Variation of shear stress with shear rate of 40%RC11 with 1 wt% binder and 0.08 wt% Na_2SiO_3

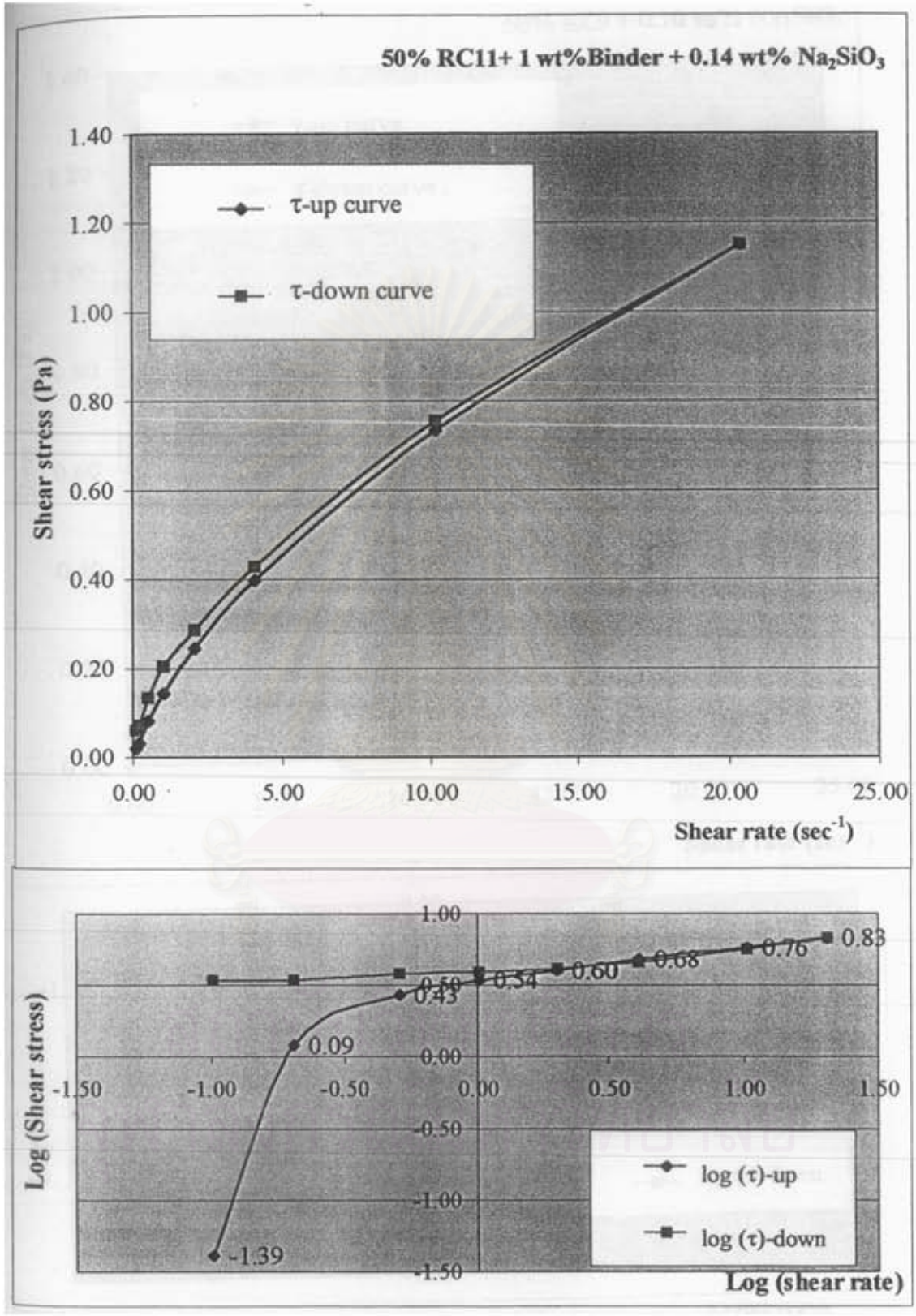

Fig. 5.20 Variation of shear stress with shear rate of 50%RC11 with 1 wt% binder and 0.14 wt% Na_2SiO_3

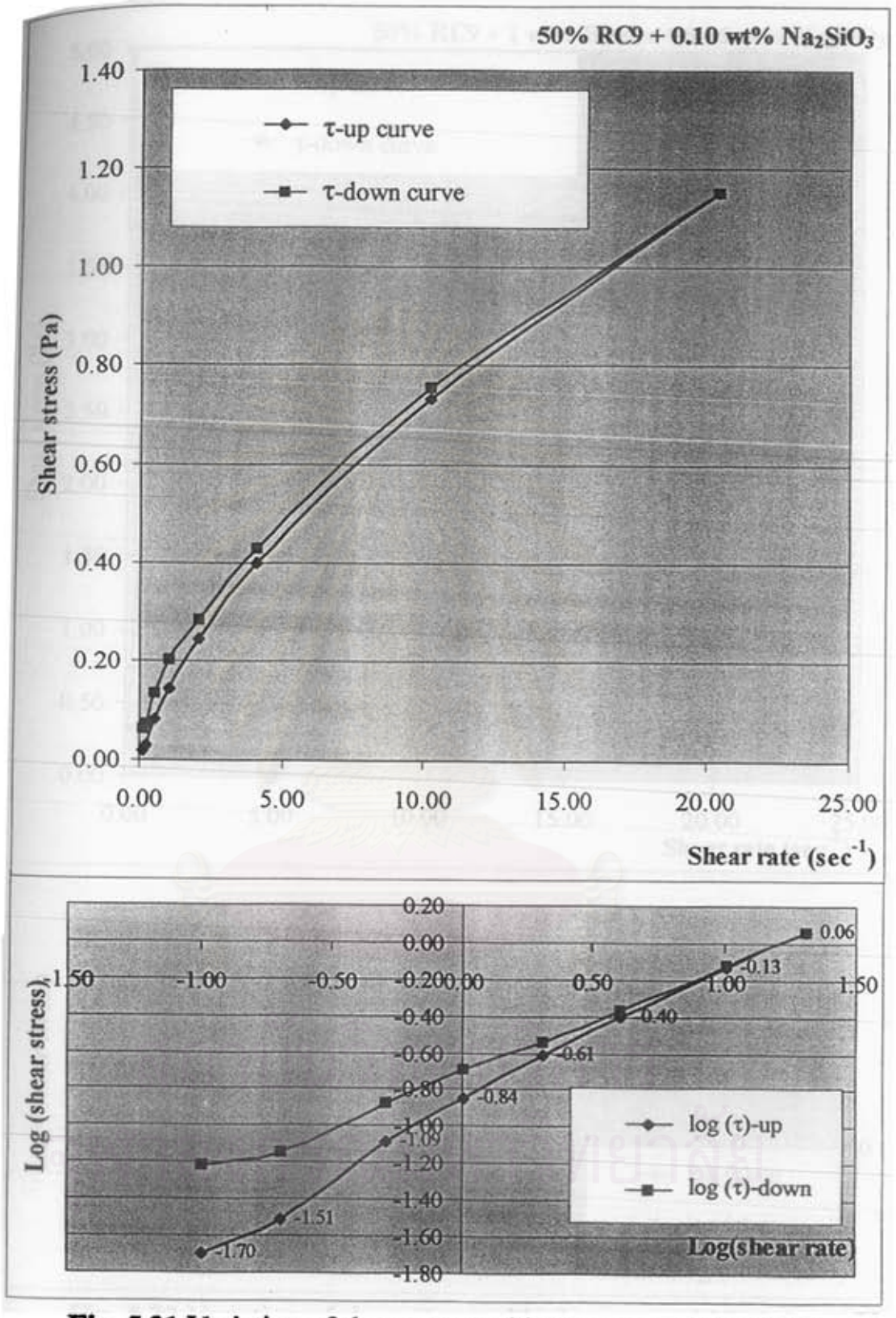

Fig. 5.21 Variation of shear stress with shear rate of 50%RC9 with 0.10 wt% Na_2SiO_3

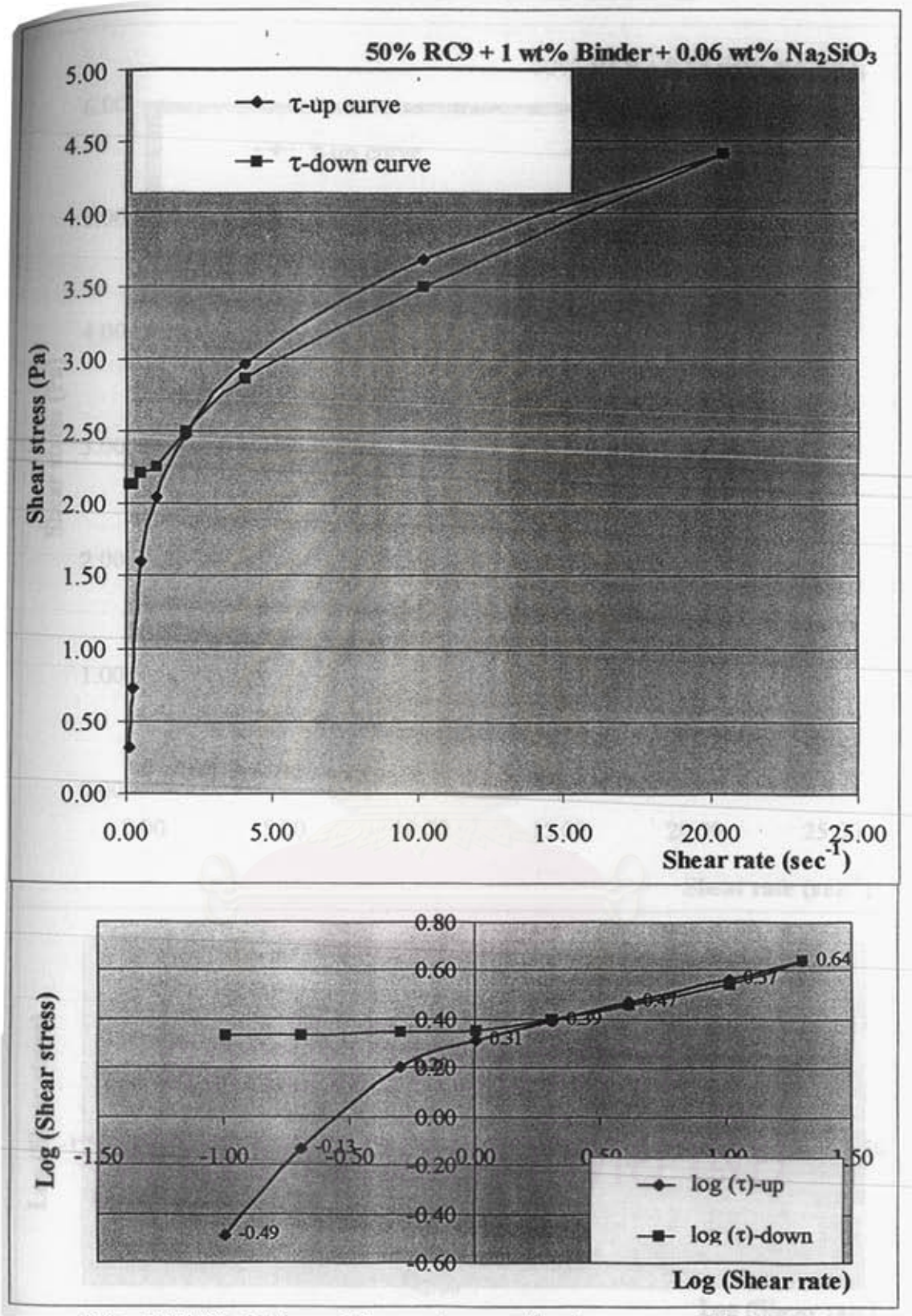

Fig. 5.22 Variation of shear stress with shear rate of 50%RC9 with 1 wt% binder and 0.06 wt% Na_2SiO_3 (partially dispersed)

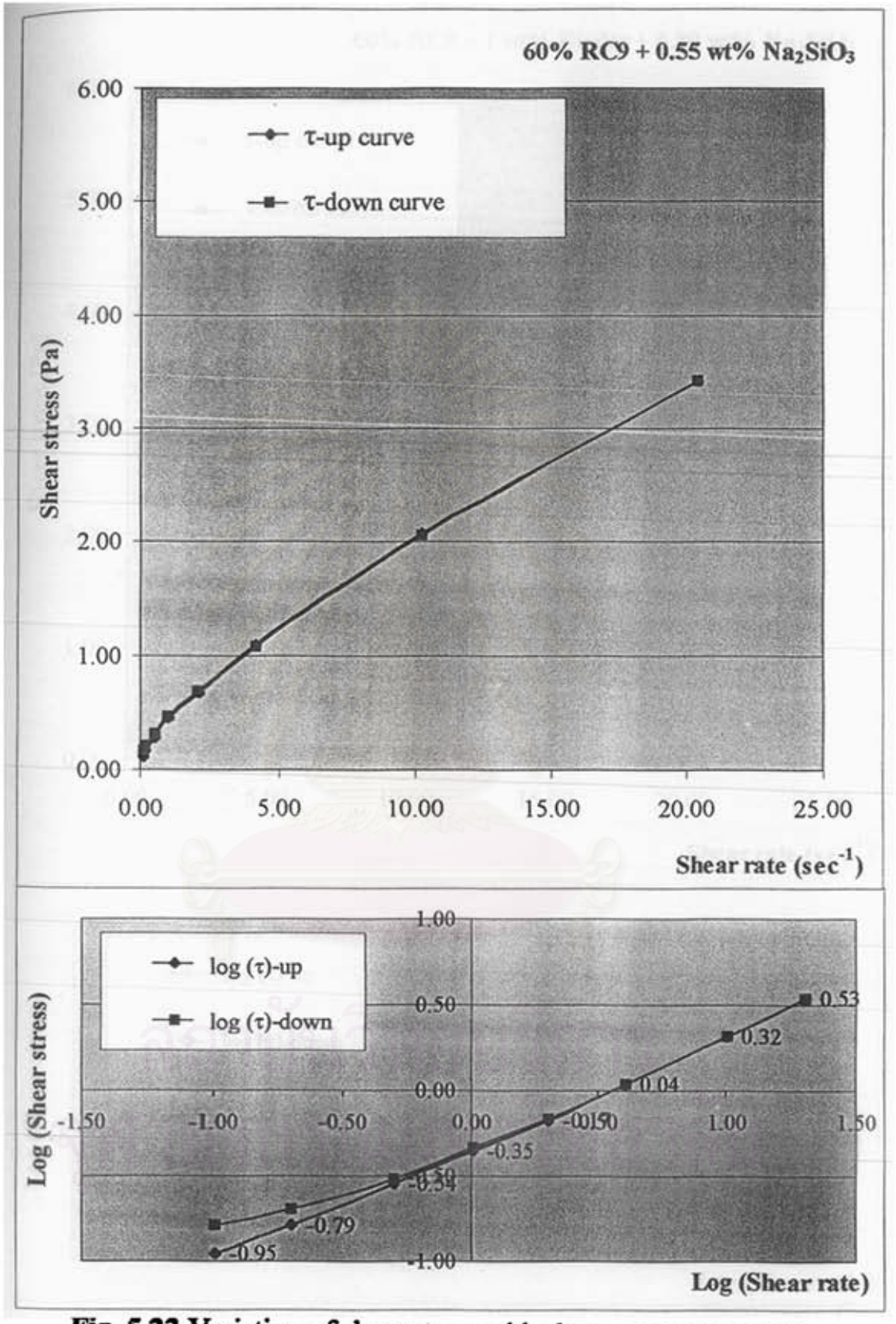

Fig. 5.23 Variation of shear stress with shear rate of 60%RC9 with 0.55 wt% Na_2SiO_3

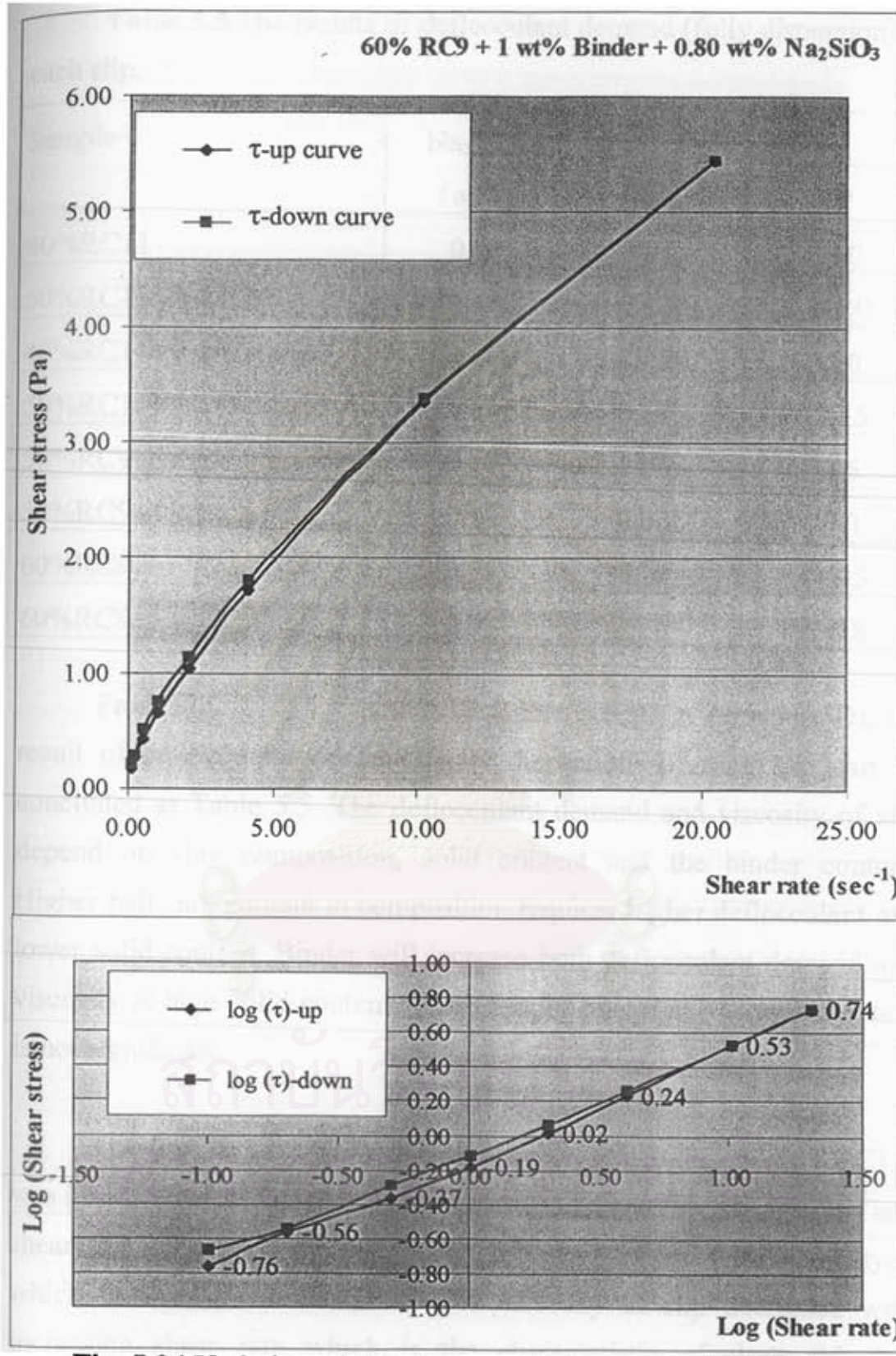

Fig. 5.24 Variation of shear stress with shear rate of 60%RC9 with 1 wt% binder and 0.80 wt% Na_2SiO_3

Table 5.5 The results of deflocculant demand (fully dispersion) of each slip.

Sample	Na_2SiO_3 (wt%)	Viscosity	
		Pa.s	cP
40%RC11	0.06	0.035	35.0
50%RC11	0.14	0.130	130.0
40%RC11+1 wt% binder	0.08	0.065	65.0
50%RC11+1 wt% binder	0.14	0.123	122.5
50%RC9	0.10	0.058	57.5
50%RC9+1 wt% binder	0.10	0.070	70.0
60%RC9	0.55	0.143	142.5
60%RC9+1 wt% binder	0.80	0.209	208.8

From Fig. 5.16, 5.17 and 5.18 (Table 2D-3D in Appendix D), the result of deflocculant demand (fully dispersion) of each slip can be concluded as Table 5.5. The deflocculant demand and viscosity of slip depend on clay composition, solid content and the binder content. Higher ball clay content in composition requires higher deflocculant and lower solid content. Binder will increase both deflocculant demand and viscosity at high solid content. The effect of binder at low solid content is not significant.

The flow behavior of the slips (except 40%RC11 and 50%RC11) was investigated and found that the relationship between shear stress and shear rate of samples shown in Fig. 5.19 to 5.24 is of the same type which is Non-Newtonian flow. The viscosity of slip decreases with increasing shear rate which is the characteristic of shear thinning behavior of Non-Newtonian liquid. After plotting the curve of log (shear stress) with log (shear rate), log (shear stress) is not proportional to log

(shear rate) for the whole range. Only at moderate shear rate, the rheology of slip will obey the power law equation (equation (4.1)). It deviates from the power law at low and high shear rate regions. This can be described as a shear thinning with time dependence or thixotropic behavior. After decreasing shear rate, the downward curve does not coincide with the upward curve, hence results in a thixotropic loop. (The data table of shear responses are in Table 4D-5D of Appendix D) In some slips, the flow type is the mixture between thixotropy (at high shear rate) and rheopectic (higher shear stress of down-curve compared with up-curve at low shear rate) as shown in Fig. 5.19 and 5.22. Although the higher shear stress of down-curve exhibits rheopectic flow by theory. Due to the true rheopectic flow is very rare to occur, the nature of flow curve may be influenced by the unsuitable shearing time (2 min) used in the experiment. Two slips, 50%RC11 with 1 wt% binder and 0.14 wt% Na_2SiO_3 (Fig. 5.20) and 50%RC9 with 0.10 wt% Na_2SiO_3 (Fig. 5.21), present rheopectic-like behavior. In the cases of 60%RC9 without binder (Fig 5.23), the flow is very close to pseudoplastic type while 60%RC9 with binder addition (Fig. 5.24) exhibits a mixed type of thixotropic and rheopectic-like flow. However it can be said that these two slips are pseudoplastic.

Generally, clay slips are thixotropic by nature because they are the mixture of various components in a wide range of particle size and shape distribution, especially the large fraction of colloidal size particle which originates the thixotropic behavior. However in the preparation of the slip for spray drying, the ideal condition is to employ a pseudoplastic system but practically a shear thinning with controlled thixotropic one can also be employed, especially for a clay-water system which requires specific size of granules. However in the preparation of the slip for spray drying, the shear rate is applied to adjust the flow as close as

possible to pseudoplastic in order to have a good flow of slip. Only 50%RC9 with 1 wt% binder (partially dispersed (Fig. 5.20) gives a pronounced yield stress which relates to a broad thixotropic loop.

From the plot of log $\dot{\gamma}$ Vs. log τ, the flow rate index (n) can be taken as the slope following the power law equation in the range of the straight line (nearly constant slope both up-curve and down-curve). 60%RC9 with and without binder addition should have good rheology for spray drying because their viscosities are suitable (70-200 cP) and their flow is close to pseudoplastic. Before spray drying, shear response of prepared slips is re-investigated and the results are in Appendix D (Fig. 1D-5D and Table 6D-8D)

Table 5.6 n and K of each experimental slip

Slip sample	n	K	Remark
40%RC11 +1wt% binder+0.08 wt% Na_2SiO_3	0.51	2.7	Thixotropic and rheopectic-like
50%RC11 +1wt% binder+0.14 wt% Na_2SiO_3	0.23	33.8	Rheopectic-like
50%RC9 0.10 wt% Na_2SiO_3	0.66	1.6	Rheopectic-like
50%RC9 +1wt% binder+0.06 wt% Na_2SiO_3 (partially dispersed)	0.25	20.8	Thixotropic (large loop) and rheopectic-like
60%RC9 +0.55 wt% Na_2SiO_3	0.67	4.4	Close to pseudoplastic
60%RC9 +1wt% binder+0.80 wt% Na_2SiO_3	0.71	6.4	Close to pseudoplastic and rheopectic-like

The n value of all samples is less than 1 which indicates pseudoplastic system. The n and K value are specific for each slip because the slip is of time dependent type therefore the n value is taken as the slope of the straight line region of the plot between log $\dot{\gamma}$ - log τ.

After slip characterization, conditions for spray drying are set into 2 conditions following Table 5.7 and 5.8

Table 5.7 Varied conditions of RC11 for spray drying

Sample	50RC11	46RC11	40RC11	50RC11	50RC11
%Na_2SiO_3	0.28	-	0.10	0.30	0.30
%Binder	-	-	1	1	2
Feed rate (ml/min)	50	50	50	50	50
Atomizer speed (rpm)	29000	21250	21250	32500	32500
Inlet/Exhaust air temp.(°C)	250/150	250/140	250/140	250/140	250/140

Table 5.8 Slip samples used for characterization and spray drying under fixed condition

Formula	40RC11 +1B	50RC11 +1B	50RC9	50RC9 +1B	60RC9	60RC9 +1B
%Solid content	40	50	50	50	60	60
%Binder (%solution wt/dry clay wt.)	1	1	-	1	-	1
%Na_2SiO_3*	0.08	0.14	0.10	0.06 Partially dispersed	0.55	0.80

* Selected from deflocculation curve (Fig.5.16 to 5.18)

5.3.3 Green strength

Green strength of RC slips before and after spray drying are observed. In the case of RC9 series, the green strength of RC9 slip without binder is lower than Hypure Vector®. Higher solid content with greater amount of deflocculant will increase strength as shown in Fig. 5.25. The strength of 60%RC9 before spray drying is almost 20% higher than that of 50%RC9. This is because Na_2SiO_3 in the slip presents the function of binder and dispersant simultaneously.[9] The binder can also increase the strength. It improves the strength of 60%RC9 (1 wt% binder) to the highest value of 6.49 MPa (6.49 MN/m^2) Although the strength after spray-drying decreases 10%, 60%RC9 can be improved to have a green strength as high as Hypure Vector®.

From the particle size distribution of RC9 slips before spray drying from Fig 5.26, it can be seen that Hypure Vector® is very fine and its average mean particle size is equal to 1-2 μm. RC9 and RC11 series have an average mean particle size of 5-8 and 4-8 μm., respectively and have less colloidal size.

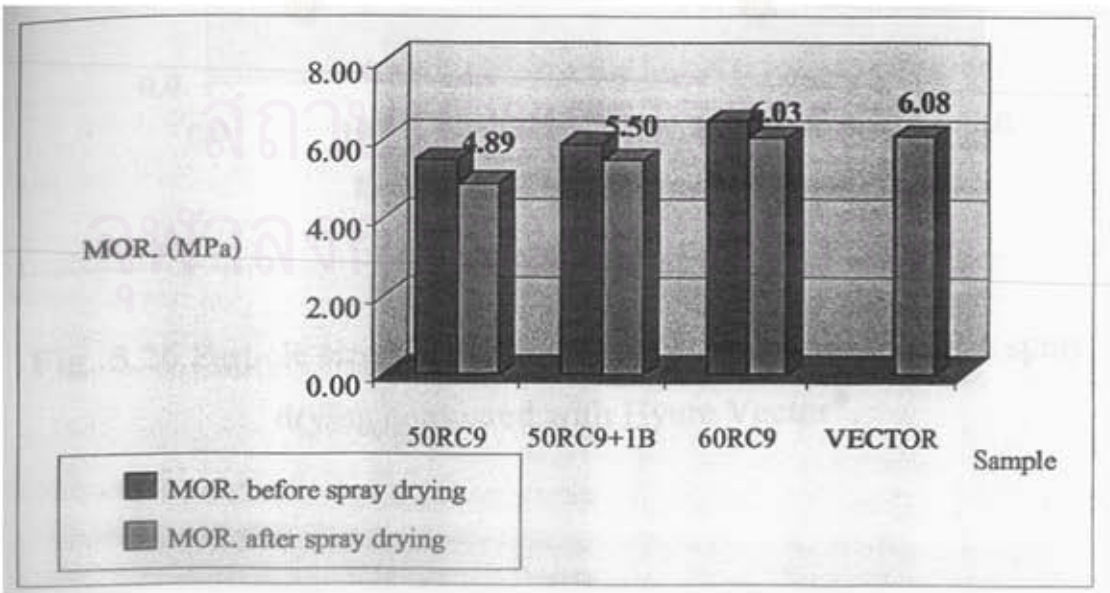

Fig. 5.25 Modulus of rupture (green strength) of RC9 slips before and after spray drying compared with Hypure Vector®.

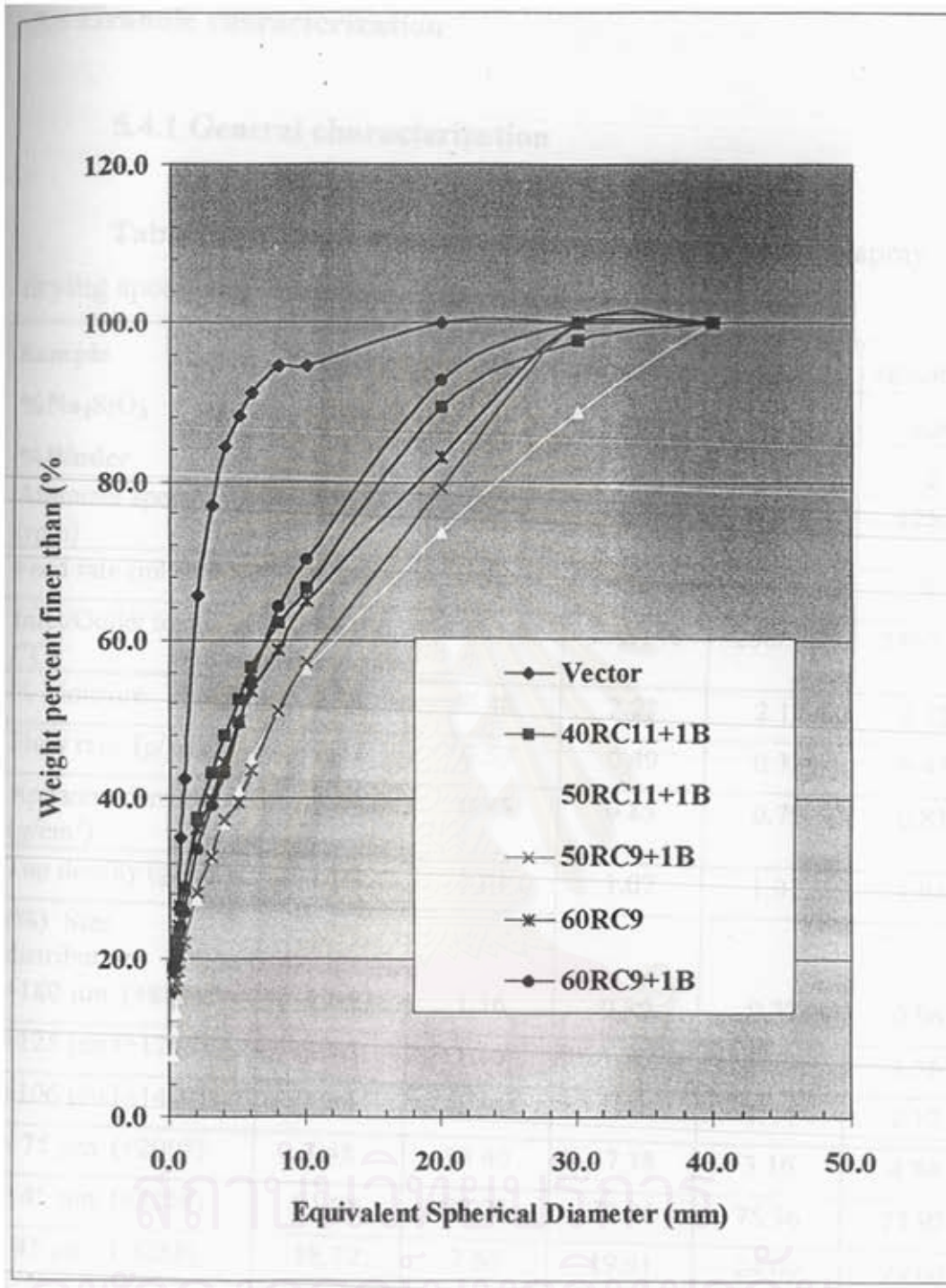

Fig. 5.26 Particle size distribution of RC slips before and after spray drying compared with Hyure Vector®.

5.4 Granule characterization

5.4.1 General characterization

Table 5.9 Flow properties of RC11 granules (Varying spray drying speed conditions)

Sample	**50%RC11**	**46%RC11**	**46%RC11**	**50%RC11**	**50%RC11**
%Na_2SiO_3	**0.28**	**-**	**0.10**	**0.30**	**0.30**
%Binder	**-**	**-**	**1**	**1**	**2**
Atomizer speed (rpm)	29000	21250	21250	32500	32500
Feed rate (ml./min)	50	50	50	50	50
Inlet/Outlet temp. (°C)	250/150	250/140	250/140	250/140	250/140
% Moisture	2.21	2.48	2.23	2.18	2.22
Flow rate (g/sec.)	0.42	0.53	0.49	0.38	0.43
Apparent density (g/cm^3)	0.83	0.85	0.85	0.79	0.83
Tap density (g/cm^3)	1.04	1.01	1.07	1.01	1.04
(%) Size distribution +180 μm (+80#)	1.04	1.16	0.89	0.72	0.96
+125 μm (+120#)	1.56	1.56	1.56	1.12	1.56
+106 μm (+140#)	1.84	1.84	1.91	1.44	2.12
+ 75 μm (+200#)	3.48	15.40	17.38	3.16	4.84
+ 45 μm (+325#)	81.08	92.28	79.96	75.56	75.92
- 45 μm (-325#)	18.72	7.60	19.91	24.00	23.60
Sum of size distribution(%)	99.80	99.88	99.87	99.56	99.52
D_{50} (Sieve analysis)	47.49	51.13	51.60	47.01	47.95
D_{50} (Microscope image)	36.67	43.78	26.85	31.77	32.22

Table 5.10 Flow properties of RC granules (Fixed spray drying condition)

Sample	**VECTOR**	**40RC11**	**50RC11**	**50RC9**	**50RC9**	**60RC9**	**60RC9**
%Na_2SiO_3		**0.08**	**0.14**	**0.10**	**0.06**	**0.55**	**0.80**
%Binder		1	1	-	1	-	1
% Moisture	2.12	1.48	1.80	0.79	0.50	0.92	3.92
Flow rate (g/sec.)	0.42	0.29	0.47	0.44	0.47	0.55	0.49
Apparent density (g/cm^3)	0.85	0.73	0.83	0.80	0.81	0.88	0.85
Tap density (g/cm^3)	1.01	0.95	1.04	1.00	1.00	1.07	1.06
(%) Size Distribution +180 μm	77.80	0.36	0.60	0.56	0.56	1.84	4.24
+125 μm	90.40	0.56	1.12	1.04	0.92	3.16	6.16
+106 μm	93.20	0.72	1.92	1.96	1.24	3.96	7.16
+ 75 μm	98.00	3.40	8.56	13.76	3.12	7.84	9.04
+ 45 μm	99.60	69.40	76.56	80.38	78.36	82.80	76.62
- 45 μm	0.16	30.16	23.12	18.90	21.20	16.64	23.23
Sum of size Distribution (%)	99.76	99.56	99.68	99.28	99.56	99.44	99.85
D_{50} (Sieve analysis)	163.54	46.55	48.72	50.28	46.81	50.22	53.45
D_{50} (Microscope image)	272.4	31.01	26.97	27.55	30.89	31.52	29.37

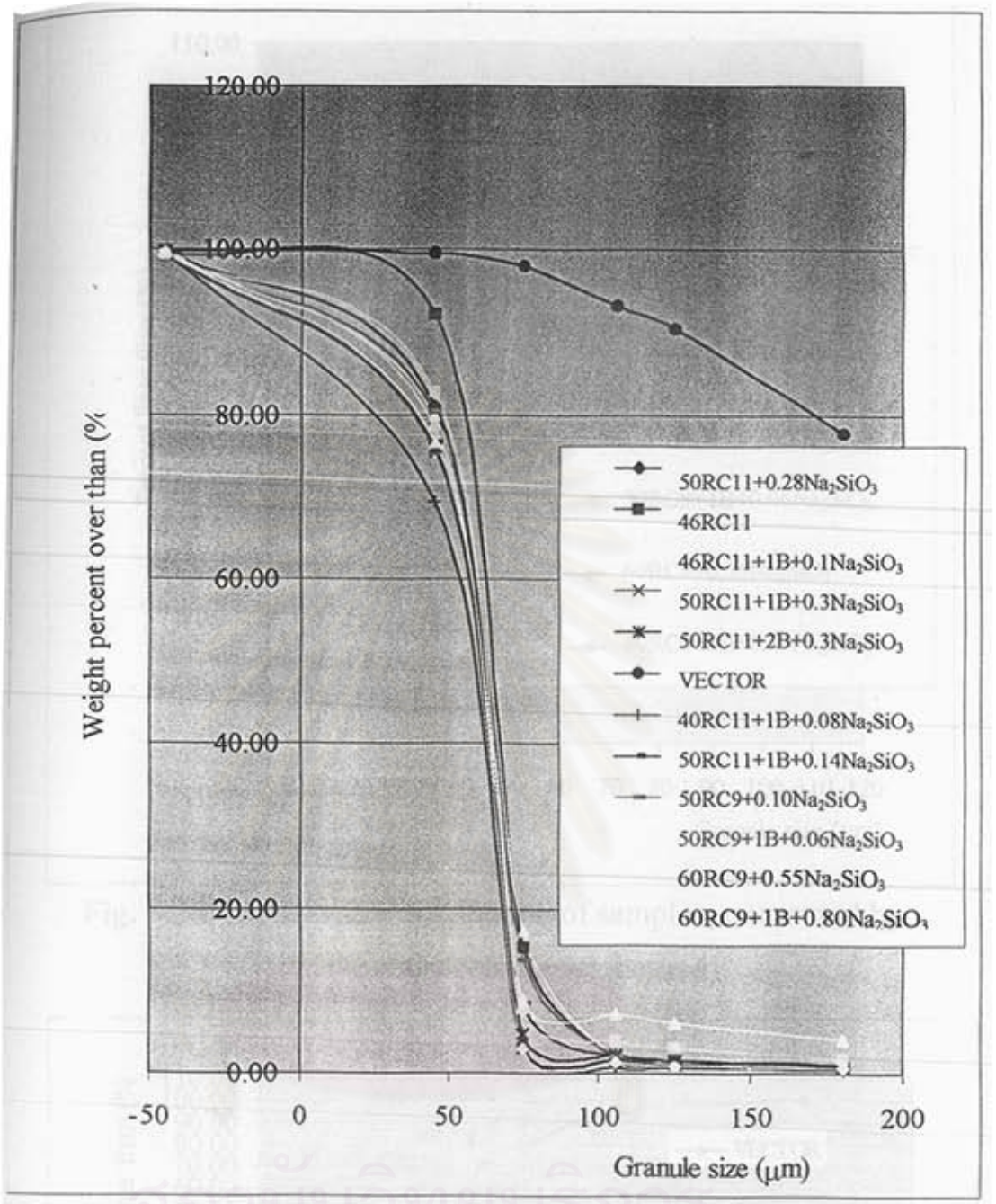

Fig. 5.27 Granule size distribution of samples by sieve analysis (data table in Appendix F- Table 1F)

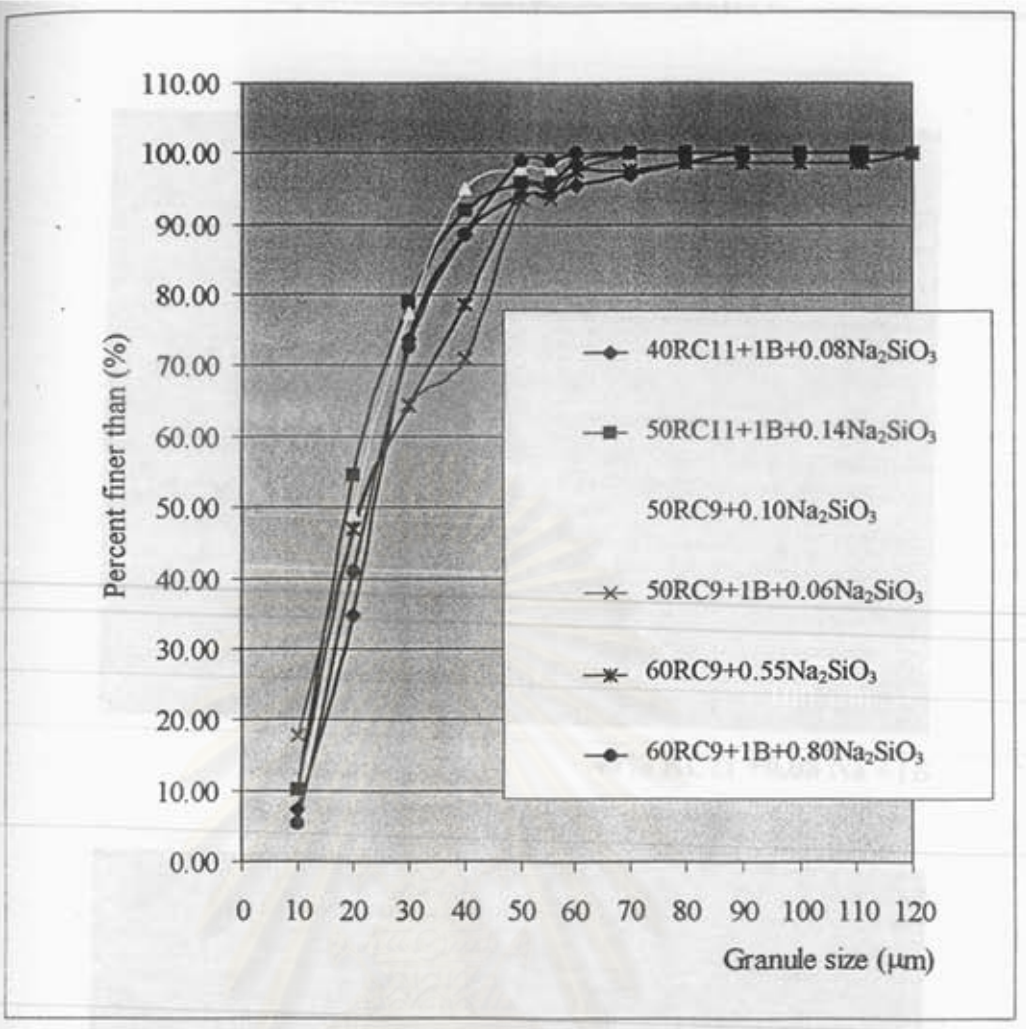

Fig. 5.28 Granule size distribution of samples, measured by stereomicroscope (Ferret method)

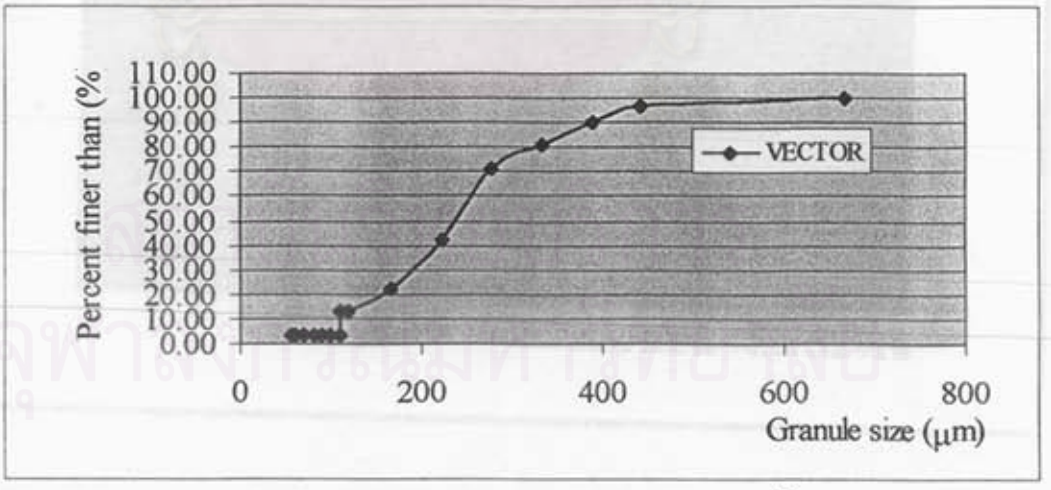

Fig. 5.29 Granule size distribution of Hyure Vector®, measured by stereomicroscope (Ferret method)
(data table in Appendix F- Table 2F)

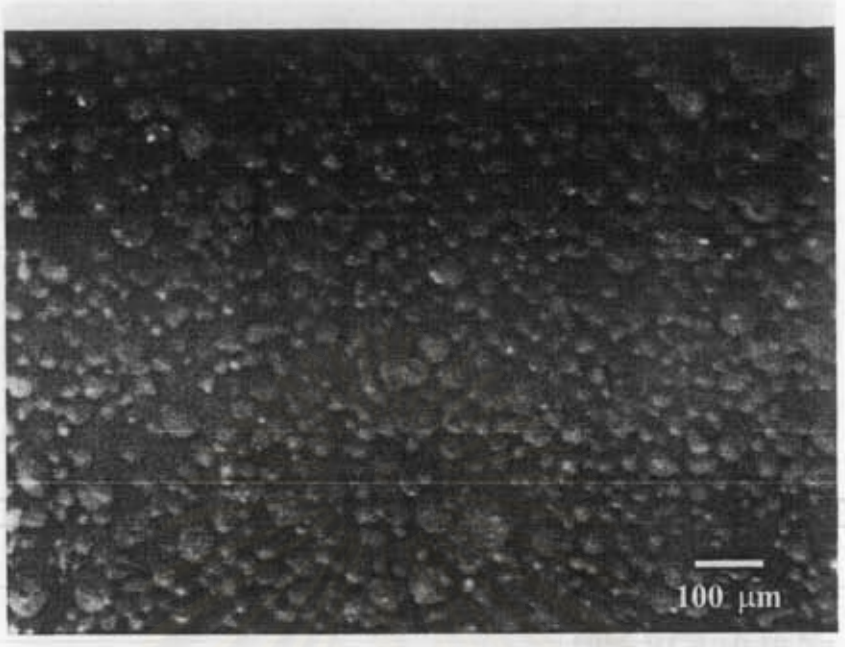

40% RC11 +0.08 Na +1B

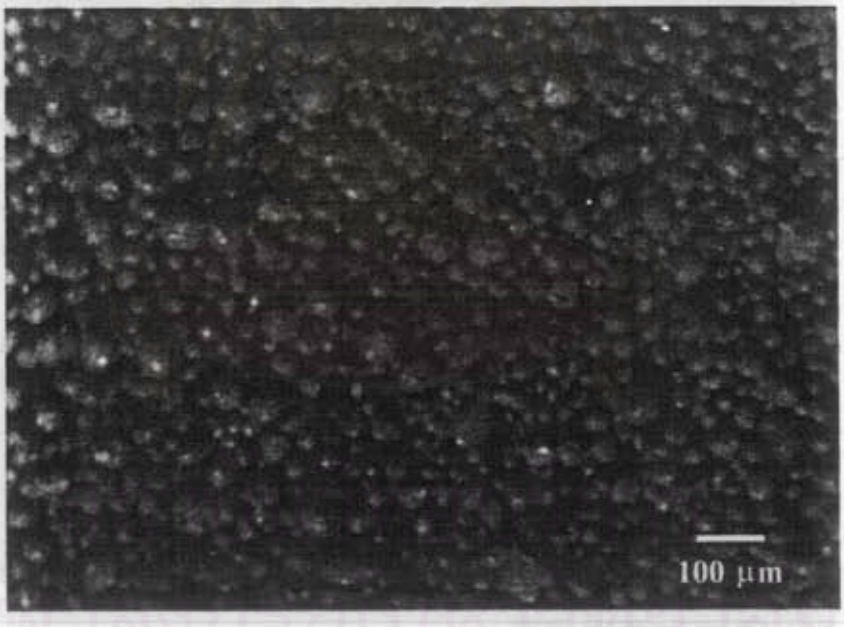

50% RC11 +0.14 Na +1B

Fig. 5.30 Granule figures of 40%RC11+1 wt% binder+ 0.08 wt% Na_2SiO_3 and 50%RC11+1 wt% binder + 0.14 wt% Na_2SiO_3 (Fixed condition) by stereomicroscope

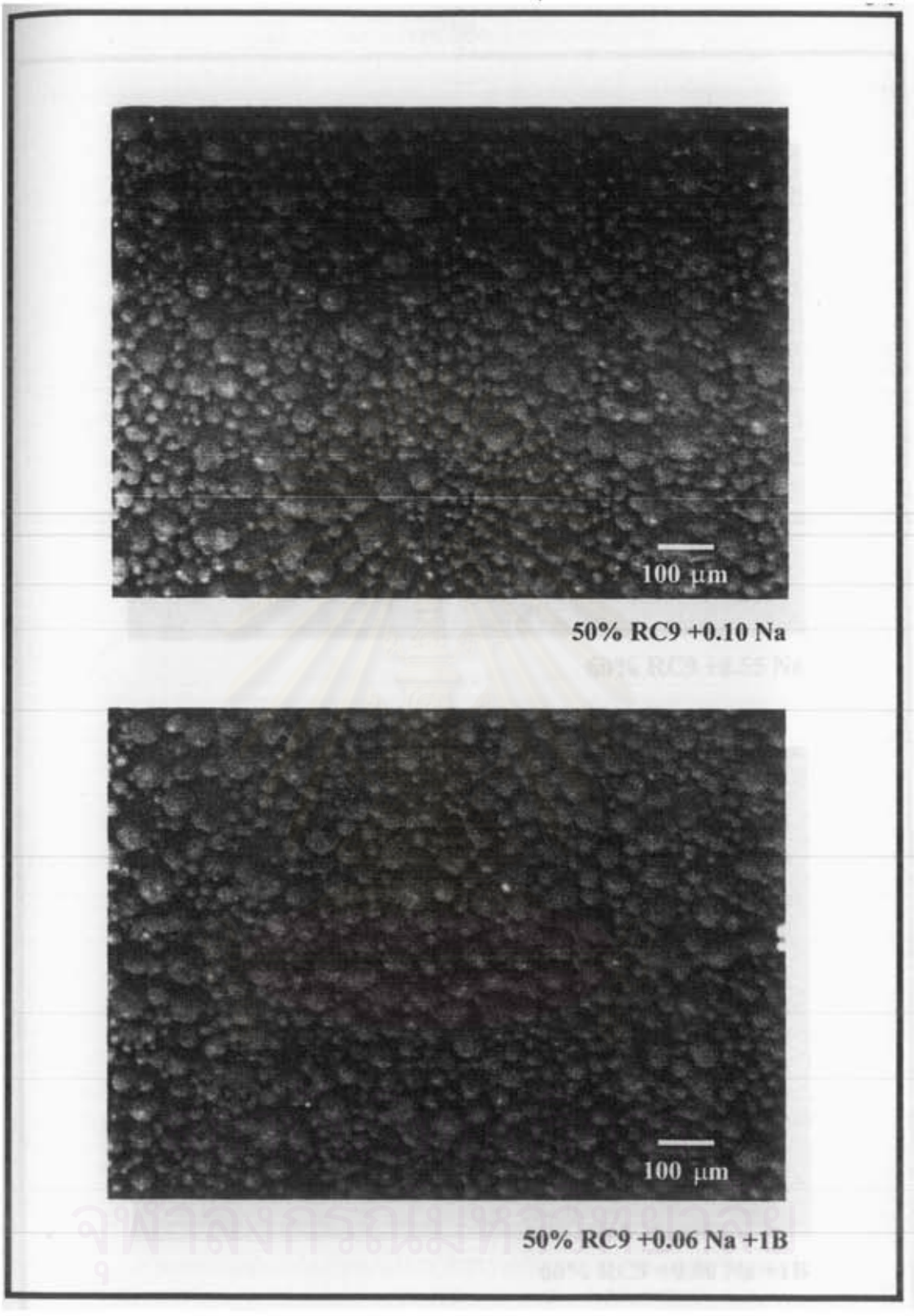

Fig. 5.31 Granule figures of 50%RC9+ 0.10 wt% Na_2SiO_3 and 50%RC9+1 wt% binder + 0.06 wt% Na_2SiO_3 (Fixed condition) by stereomicroscope

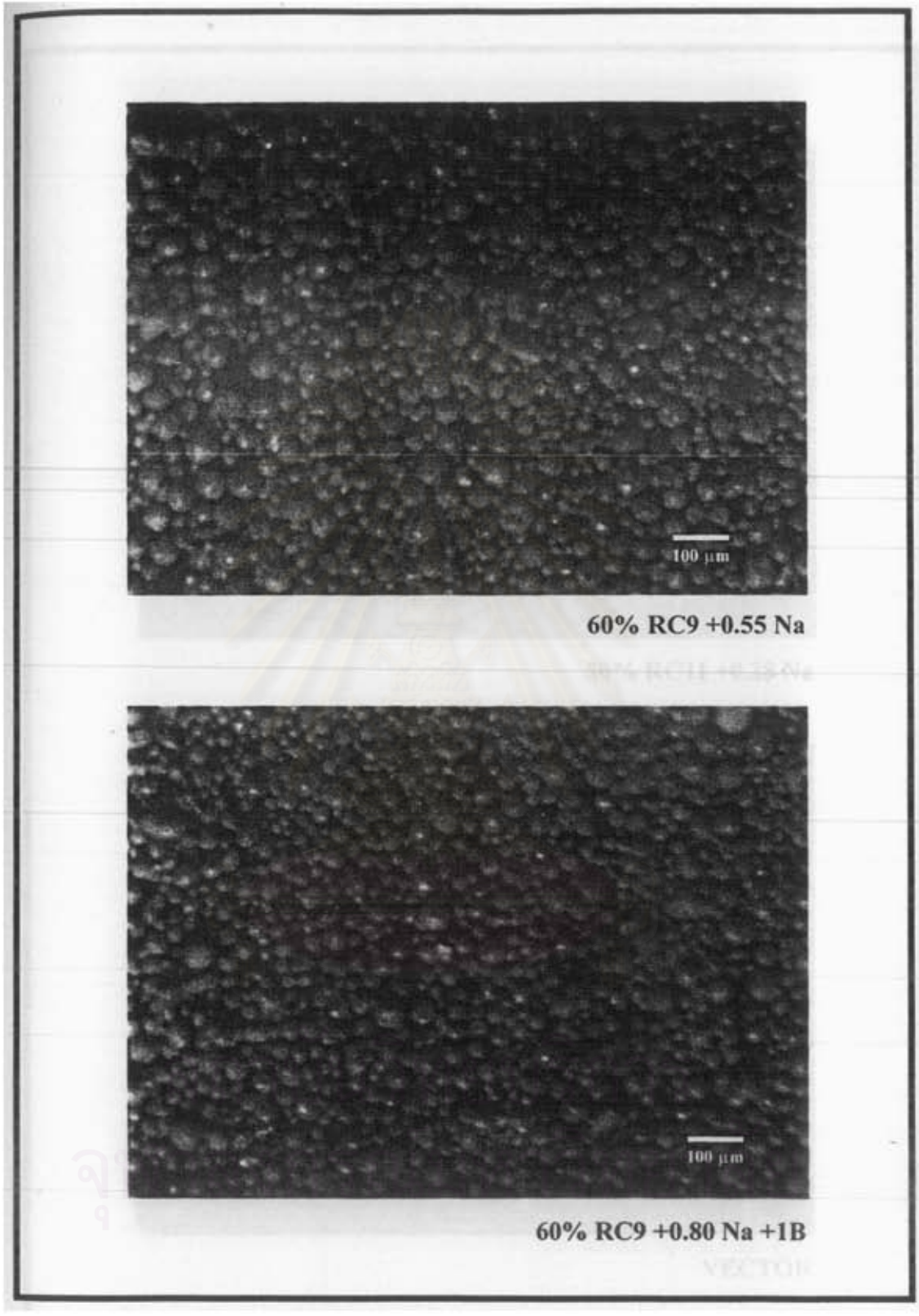

Fig. 5.32 Granule figures of 60%RC9+ 0.55 wt% Na_2SiO_3 and 60%RC9+1 wt% binder + 0.80 wt% Na_2SiO_3 (Fixed condition) by stereomicroscope

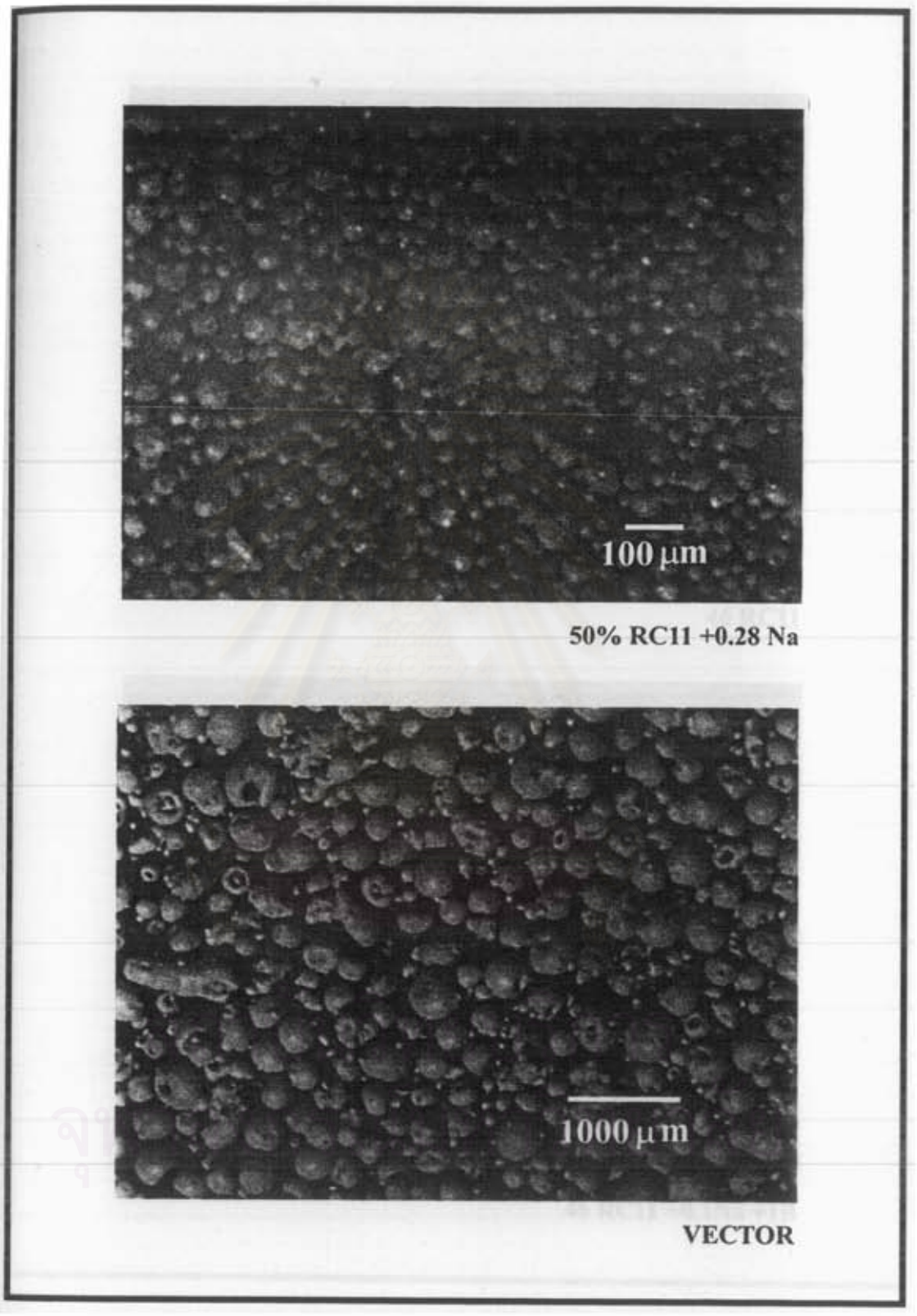

Fig. 5.33 Granule figures of 50%RC11+ 0.28 wt% Na_2SiO_3 (Varied condition) and Hypure Vector® by stereomicroscope

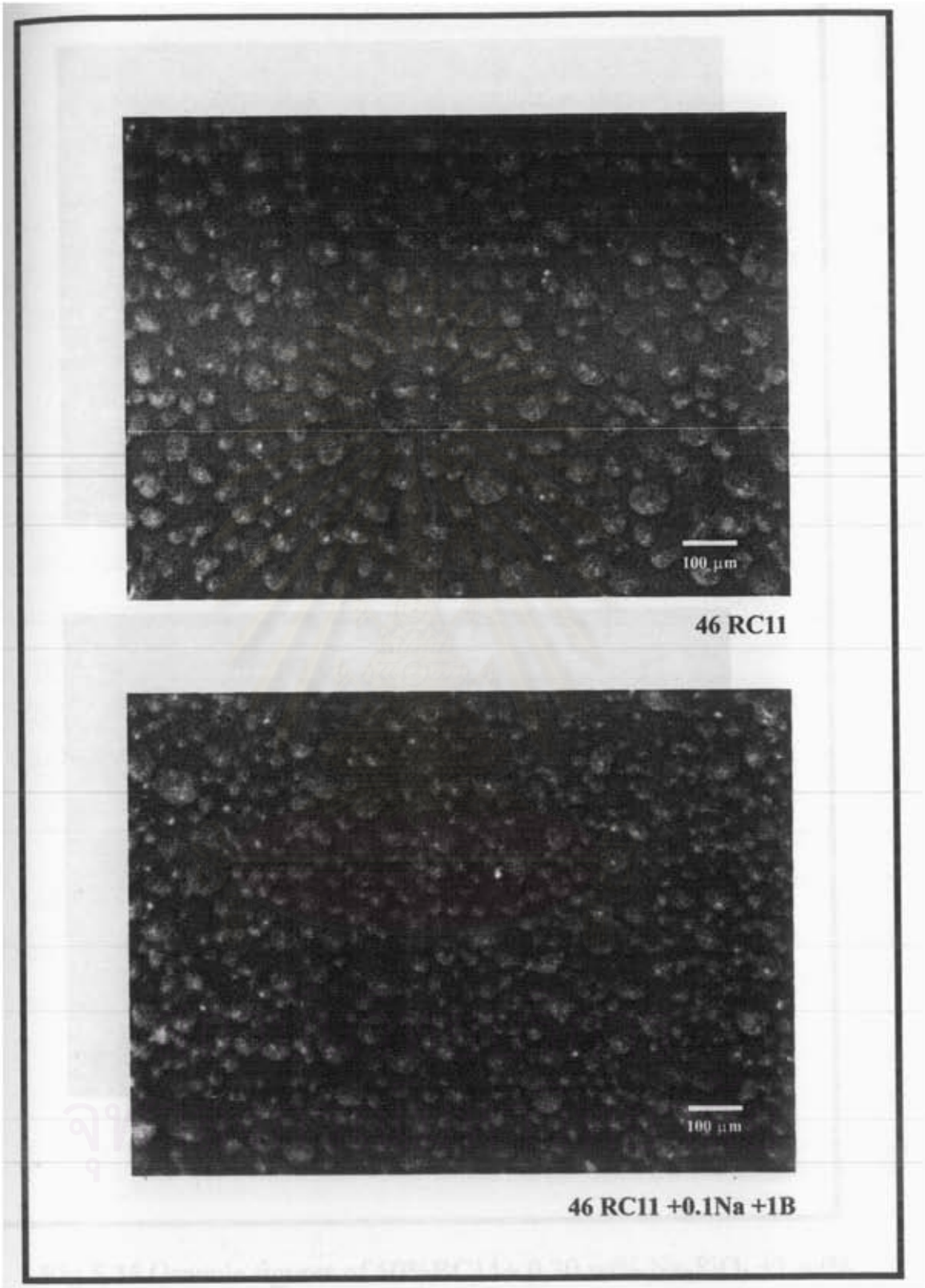

Fig. 5.34 Granule figures of 46%RC11 and 46%RC11+1 wt% binder + 0.10 wt% Na_2SiO_3 (Varied condition) by stereomicroscope

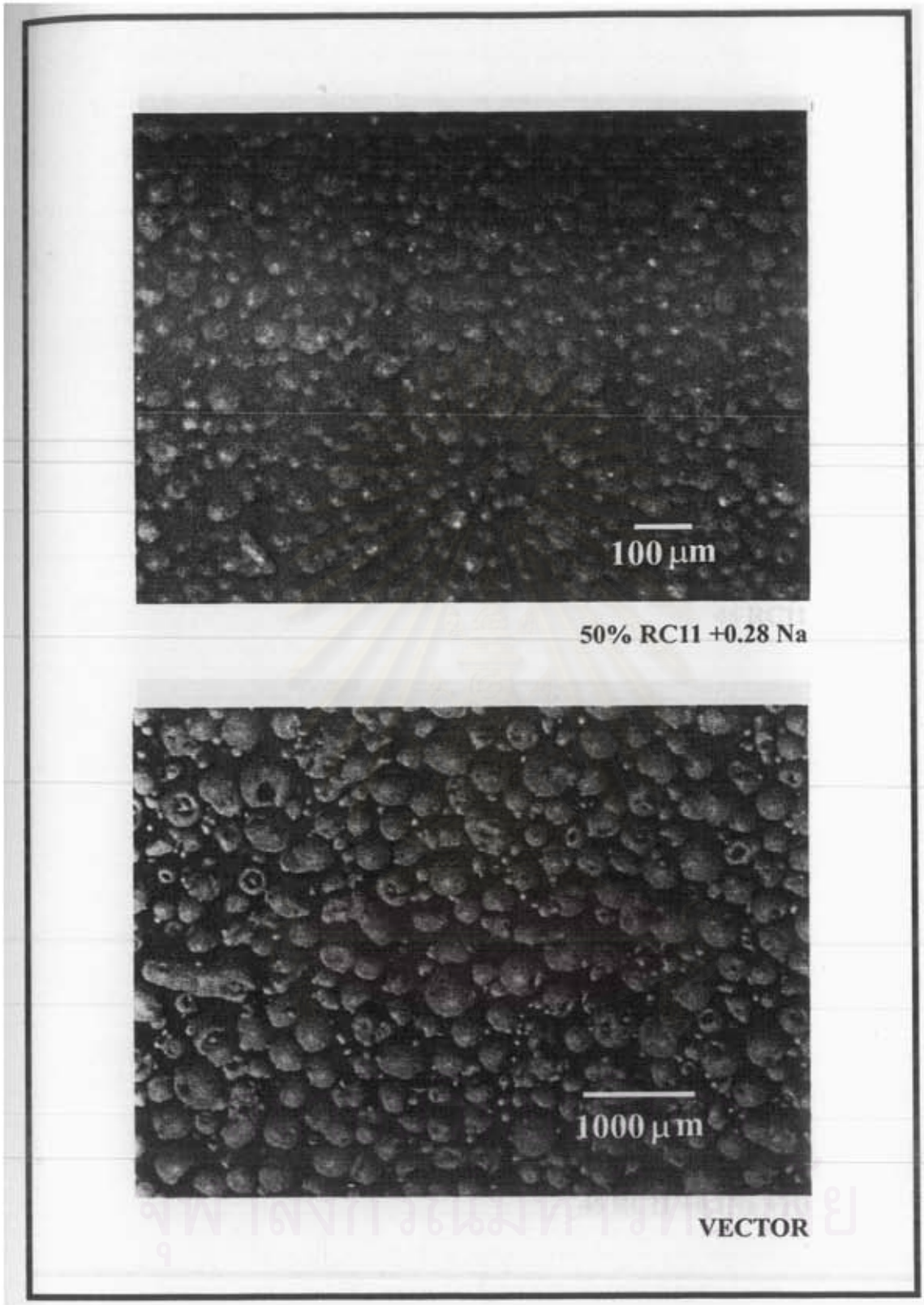

Fig.5.35 Granule figures of 50%RC11+ 0.30 wt% Na_2SiO_3 +1 wt% binder and 46%RC11+ 0.30 wt% Na_2SiO_3 + 2 wt% binder (Varied condition) by stereomicroscope

Granules received from these studies give two sets of result. Table 5.9 is the result of varying spray drying condition and Table 5.10 is the result of fixed condition. The best condition for granule character is RC9 at 60 wt% solid and 0.55 wt% Na_2SiO_3 since it has highest flow rate, 0.55 g/sec, highest apparent density, 0.88 g/cm^3, and tap density, 1.07 g/cm^3. However the values of the average mean size (D_{50}) from sieve analysis and from stereomicroscope measurement are not so close which may due to the deviation from spherical shape of the granules.

To compare the condition of spray drying from Table 5.9, granules by means of reducing atomizer (21,250 rpm.) speed have bigger size, higher flow rate (0.25-0.27 sec.), higher apparent density (0.85 g/cm^3) the trend of higher tap density. Average mean size is 51-52 μm from sieve analysis while average mean size by stereomicroscope is not representative which may come from the size of sampling test is very small compared with sieve analysis.

To consider the effect of solid content in Table 5.10, high solid content results in the high apparent and tap densities. Besides flow rate is much better. The effect of binder on granule property is that the binder can increase the granule size if slip is in fully dispersed condition. 50%RC9 with 1 wt% binder, partially dispersed, while spray drying, caused the wall deposit and clogging of the aperture of atomizer.

The moisture content of all samples are less than 4%. In addition, the interval time during spray drying may affect the moisture content. The RC9 formulas are prepared in the bigger batch and their granules are in the bottom of drying chamber for a long period, the moisture contents are less. RC9 60 wt% with 1 wt% binder (the last formula) has the highest moisture content because it has the wall deposit effect. The

droplet has less dry period, distance between atomizer in the center top of the chamber to the wall size is shorter so the droplet hits crusts on the wall before fully drying and drops to collector in the bottom. Particle size of the last one seems to have the proportion of bigger size larger than others.

From these results, the best granules (60%RC9 with 0.55 wt% Na_2SiO_3) and the worst granules (40%RC11 with 1 wt% binder and 0.08 wt% Na_2SiO_3) are detected (in dry pressing) for their property compared with other formulas (except granules from Table 5.9).

5.4.2 Workability of granule on dry pressing

From compaction testing, 50%RC9 (Fig. 5.36) with binder addition deforms at 11 MPa (compared with 50%RC9 without binder (Fig. 5.37) which deforms at 9 MPa. Whereas the granules of Hypure Vector® are very strong and maintain the granule sphere until 13 MPa. Those are the effect of the binder and granule size. In the case of binder addition, the granules are toughened so they require higher pressure to deform. Since Hypure Vector® are from spray drying with mixed-flow and nozzle atomization at higher temperature (>250°C)[26], its granule is larger and stronger than the prepared ones (spray drying with co-current and centrifugal atomization) and the binder may have been used in Hypure Vector® slip to induce the hard surface from binder migration.

The fine granules need lower pressure to compact. As the finer granules normally face the lamination effect at high pressure because of poor flowability. RC samples exhibited lamination at a pressure of 13 MPa and slightly at 11 MPa, tested on the plane normal to pressure

direction. The lamination effects of 60%RC9 and 40%RC11 with 1 wt% binder are shown in Fig. 5.41 and in Appendix F (Fig. 4F), respectively. Other samples give the same results as also shown in Appendix F.

Green density of the samples depends on the applied pressure and formula. The higher pressure, the higher density because of the close packing. 60%RC9 with 1 wt% binder has the highest green density. Due to high moisture of 60%RC9 with 1 wt% binder may increase the green density because the moisture can lubricate the granule and soften the granule to break easily. 50%RC9 has the green density nearly equivalent to Hypure Vector® (Fig. 5.42).

For the fired properties, the samples pressed at higher pressure trend to have less firing shrinkage (Fig. 5.43). The weight loss is not significantly different, except RC11 at high pressure which showed black core after firing due to the organic matter content in RC11 formula (based on percentage of BCW) is higher than RC9 and the organic carbon cannot be entirely released from the densed sample at the same firing condition with the others. This can be solved by adjusting the firing condition to be slower than normal for the samples pressed at high pressure.

The chemical composition of Hypure Vector® with higher flux content (Table 5.1) causes the high shrinkage and density which effects firing properties in the way that its water absorption and bulk density are not so sensitive to applied pressures compared with RC9 and RC11. However disadvantage of higher flux content with TiO_2 is reducing the whiteness.

From all of workability results, 40%RC11 has the nearest properties to Hypure Vector® but whiter color, higher water absorption (1.36-4.11%) and a little bit lower bulk density (2.23-2.44 g/cm^3). 60%RC9 has the compaction behavior better than the others, higher green density (1.78-1.90 g/cm^3) because of high solid content, no addition of binder and the best flow rate. The firing properties of RC9 are the best, brightest color, lower shrinkage and higher water absorption.

After firing, both RC9 and RC11 have mullite and sillimanite phases[27,28] at 1200°C but sillimanite is not detected in Hypure Vector®. At higher temperature, 1245°C, the content of sillimanite in both samples decreases because it decomposed to mullite and SiO_2.(Fig. 5.46)

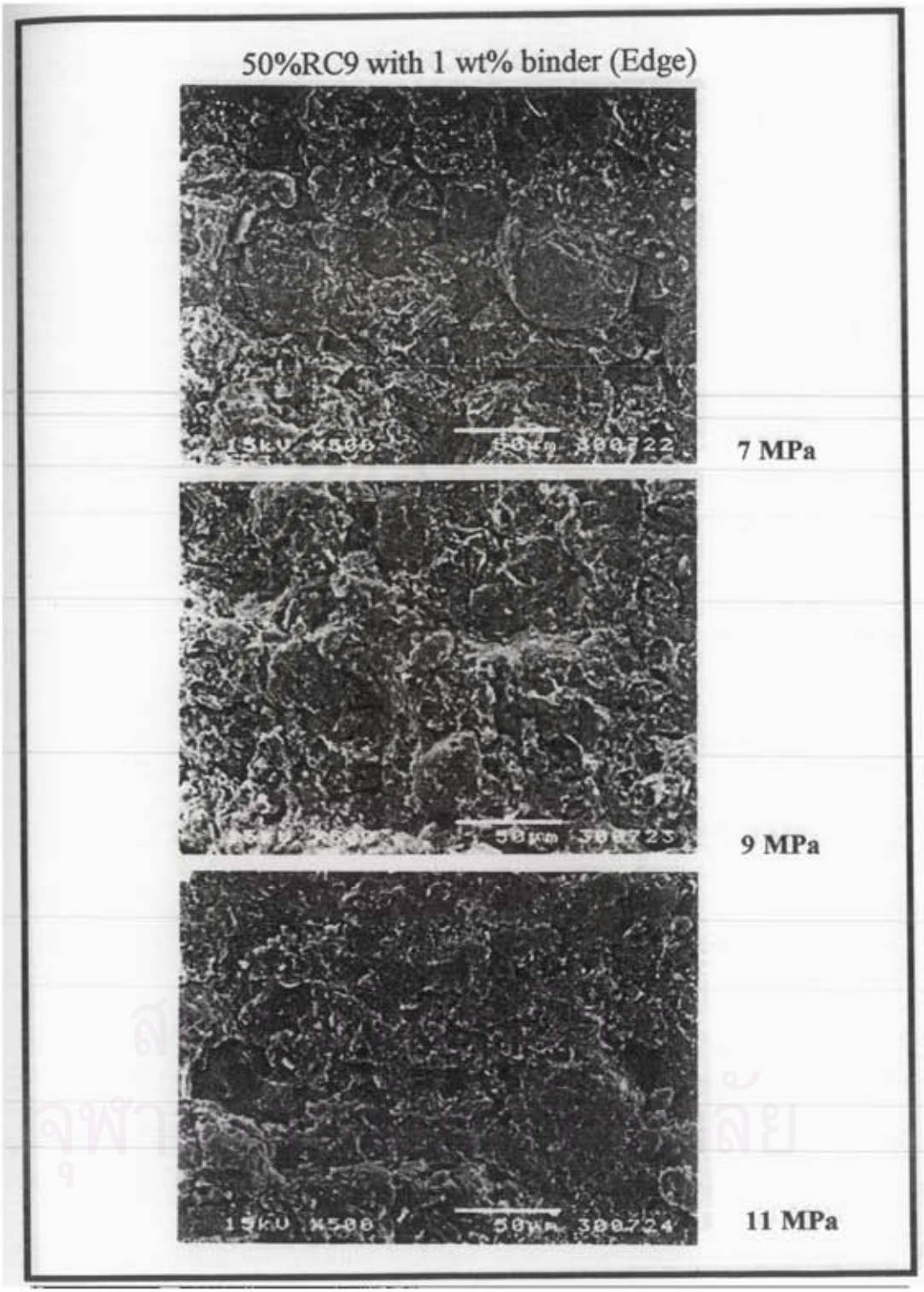

Fig. 5.36 Granule deformation of 50%RC9 with 1 wt% binder at various pressures (Fracture surface by SEM x 500)

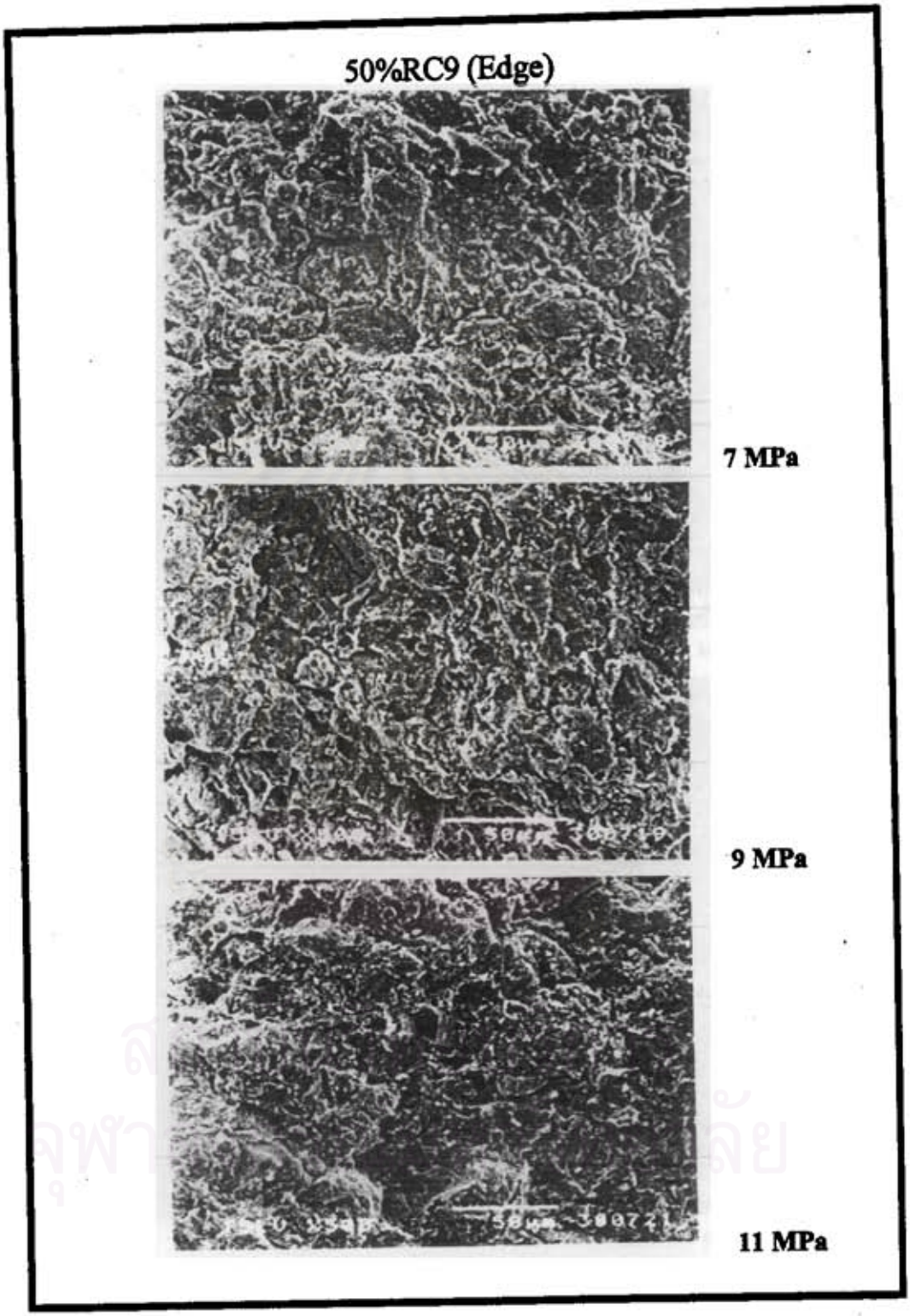

Fig. 5.37 Granule deformation of 50%RC9 without binder at various pressures (Fracture surface by SEM x 500)

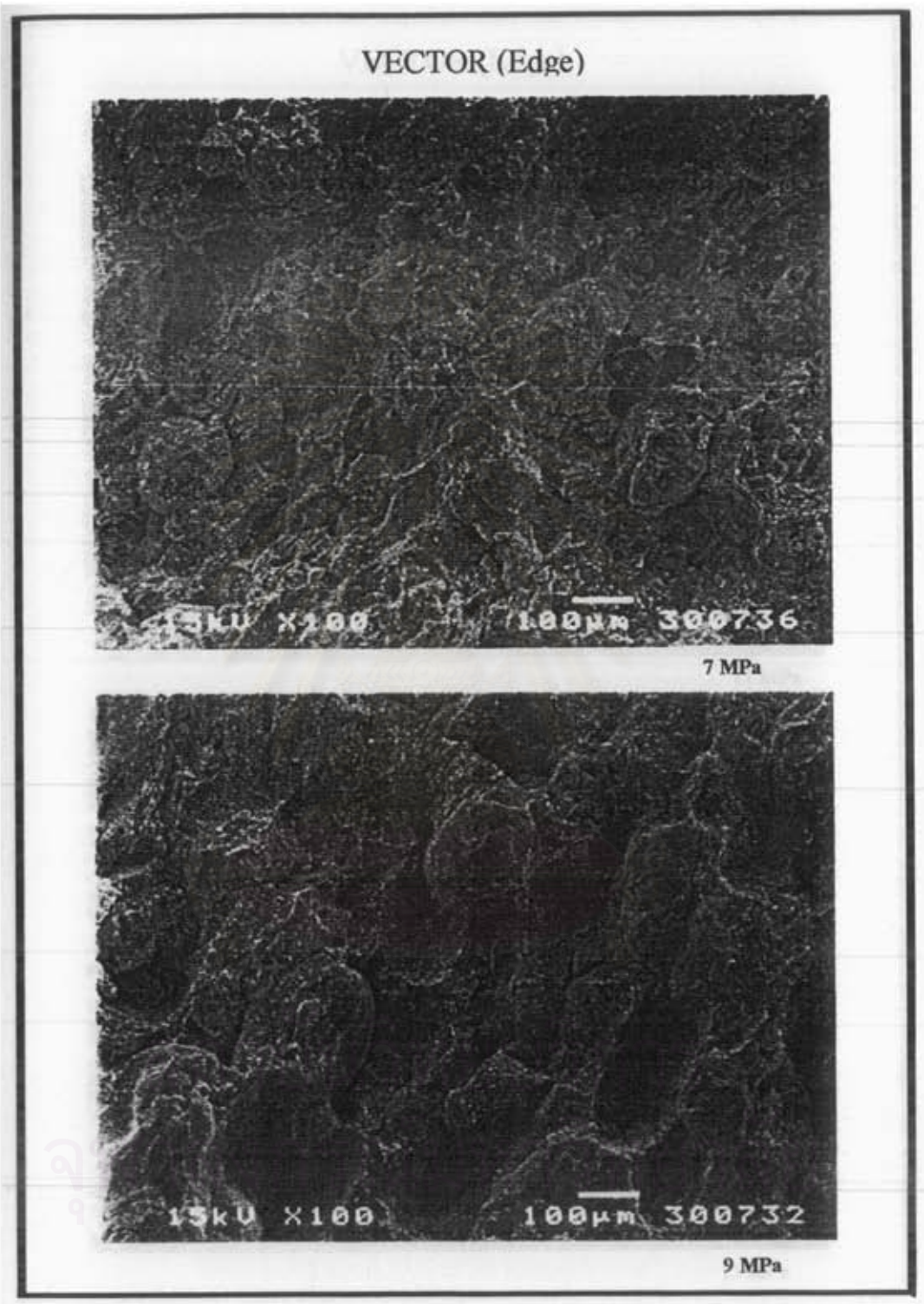

Fig. 5.38 Granule deformation of Hypure Vector® at various pressures – 7 and 9 MPa (Fracture surface by SEM x 500)

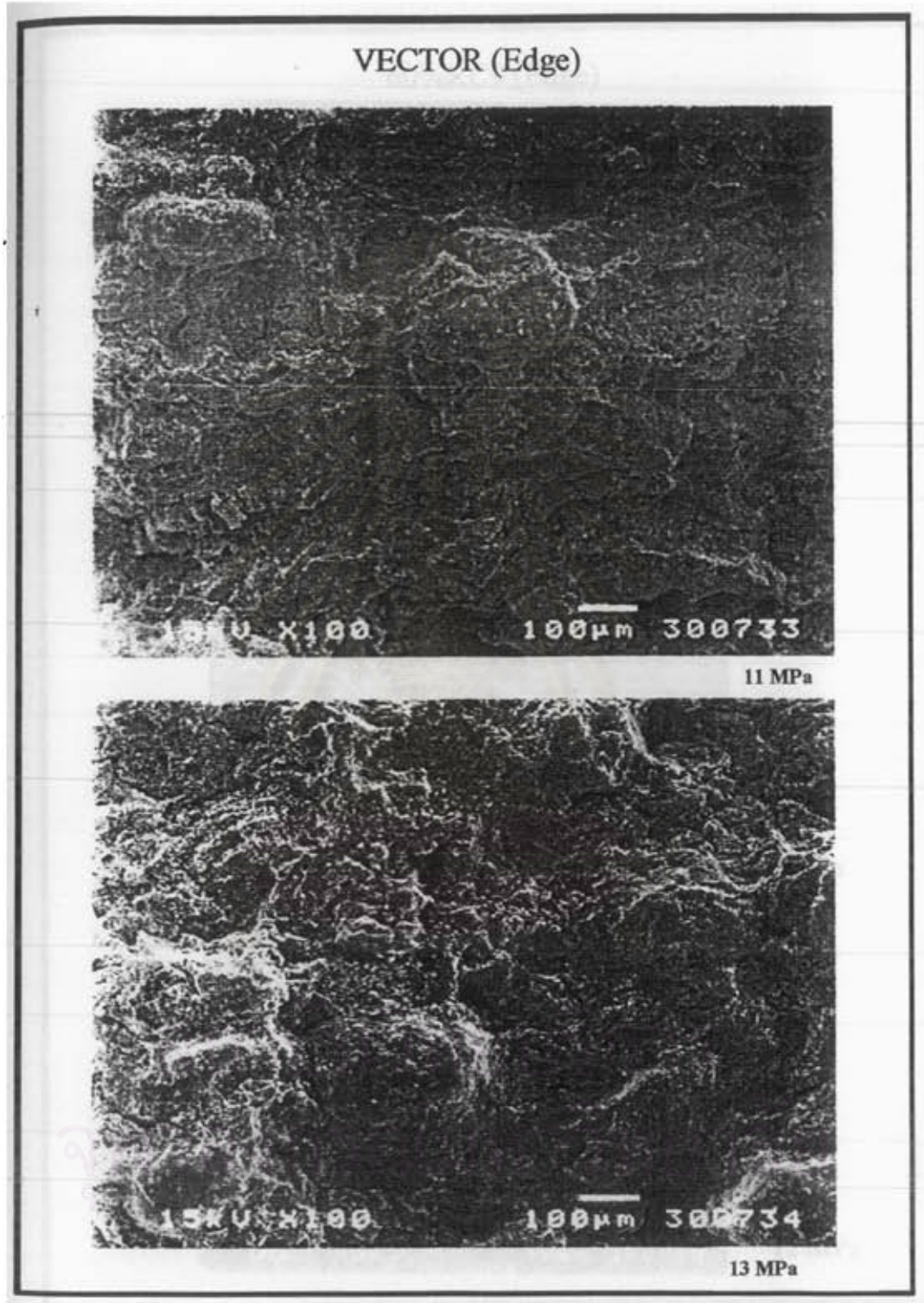

Fig. 5.39 Granule deformation of Hypure Vector® at various pressures – 11 and 13 MPa (Fracture surface by SEM x 500)

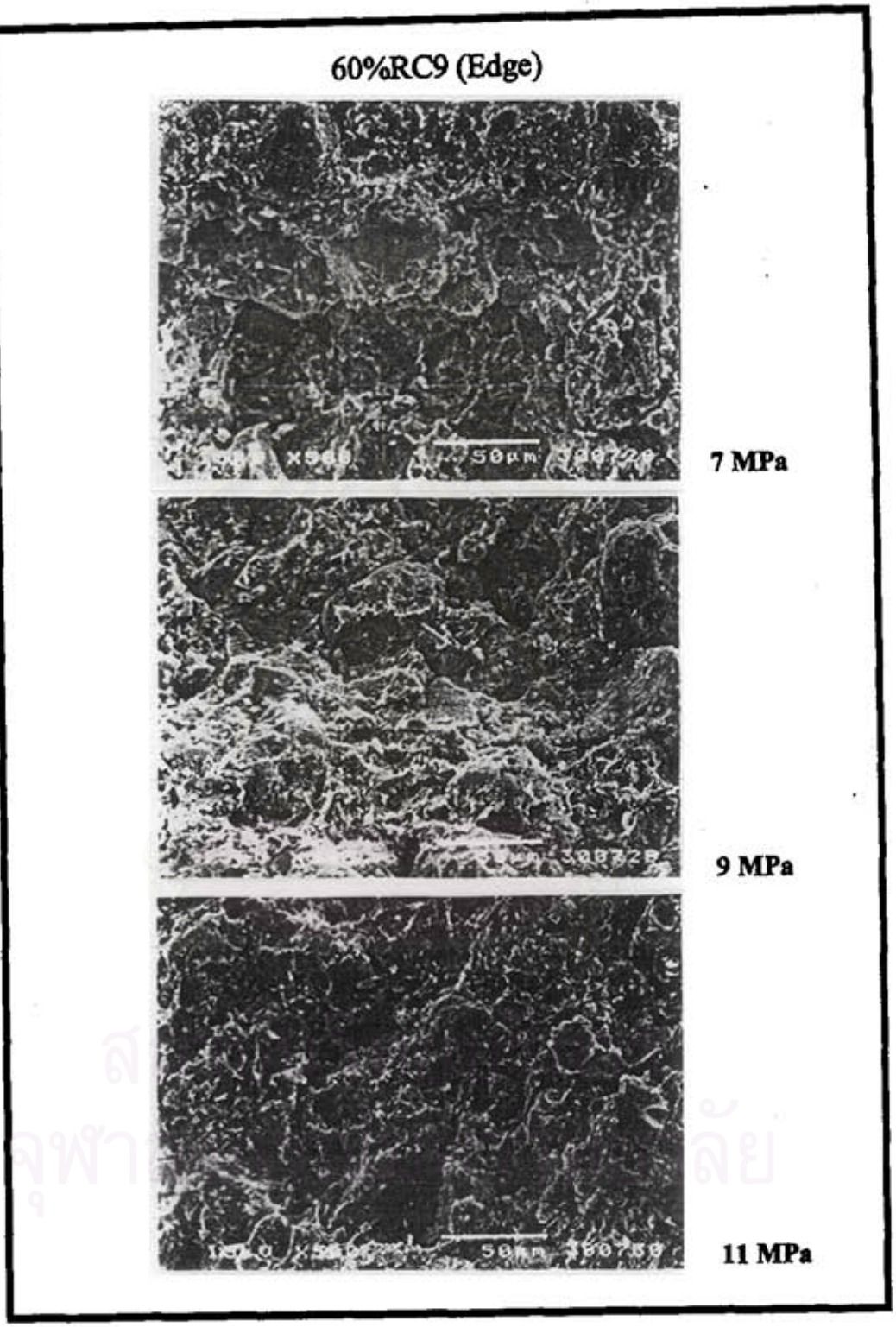

Fig. 5.40 Granule deformation of 60%RC9 without binder at various pressures (Fracture surface by SEM x 500)

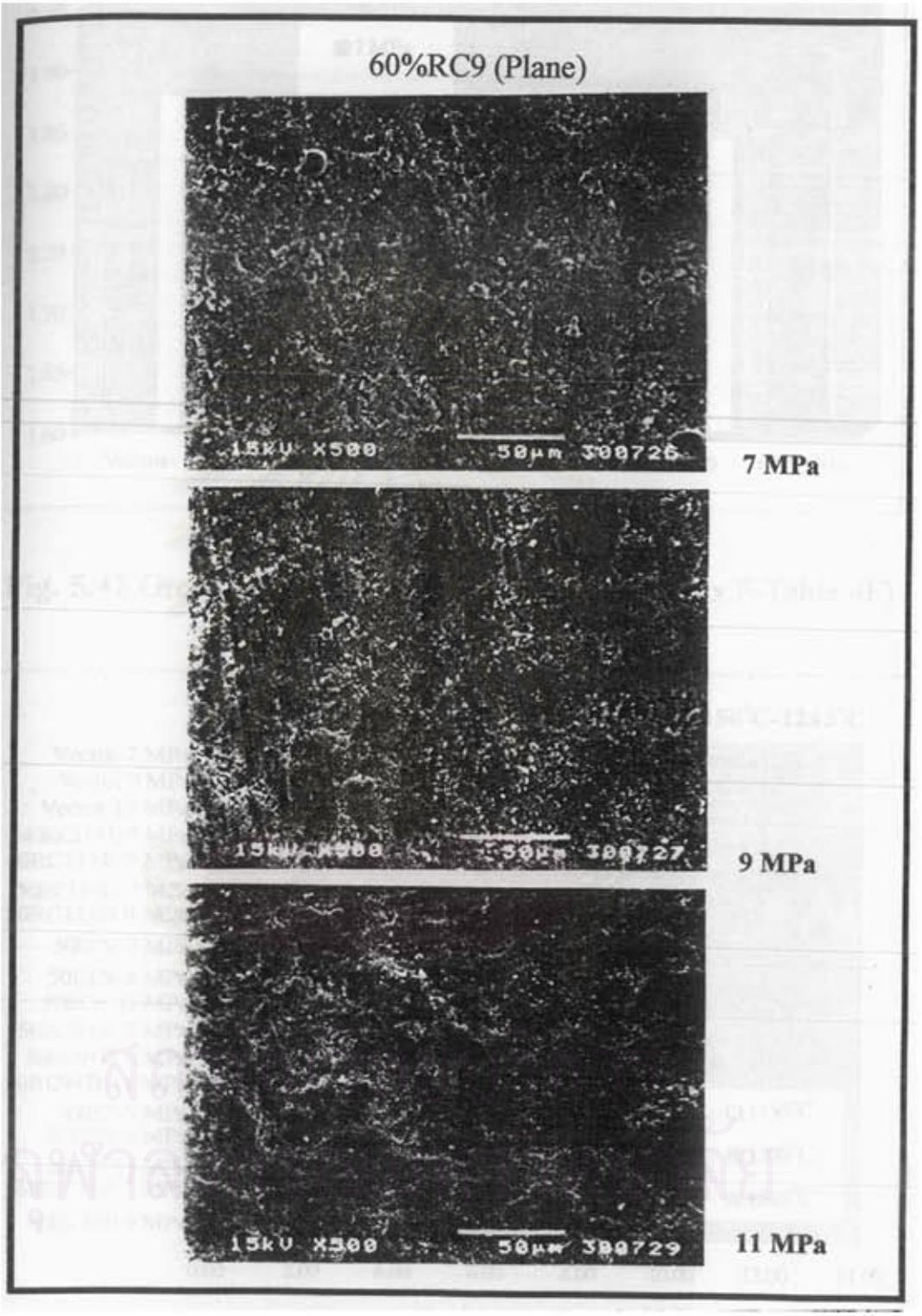

Fig. 5.41 Surface of 60%RC9 without binder at various pressures (SEM x 500)

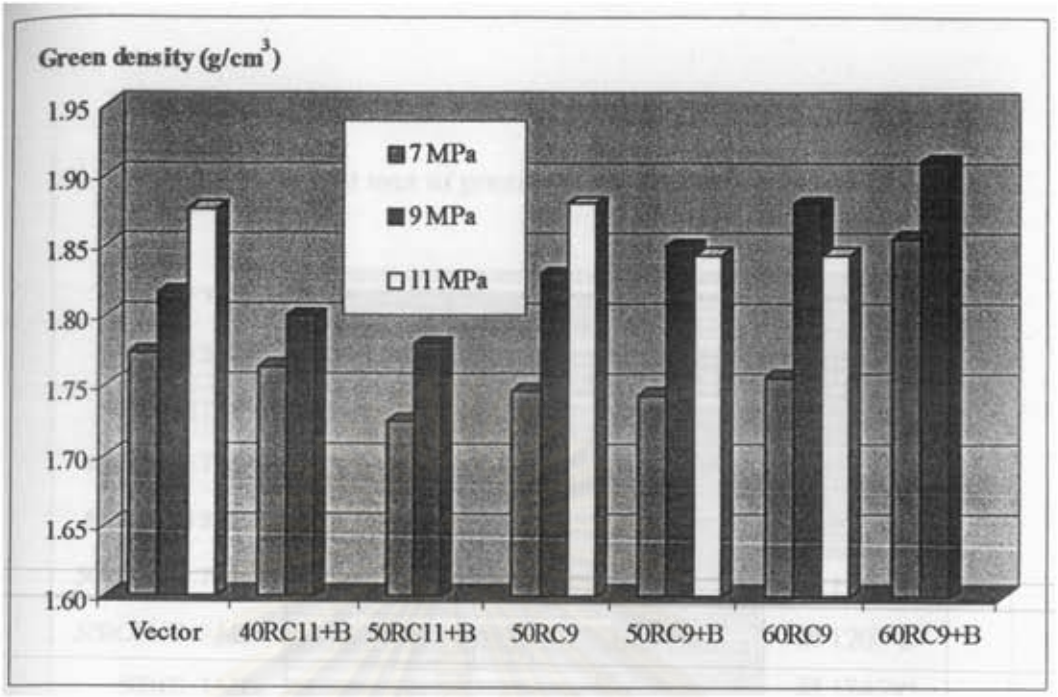

Fig. 5.42 Green density of pressed samples. (Appendix F-Table 4F)

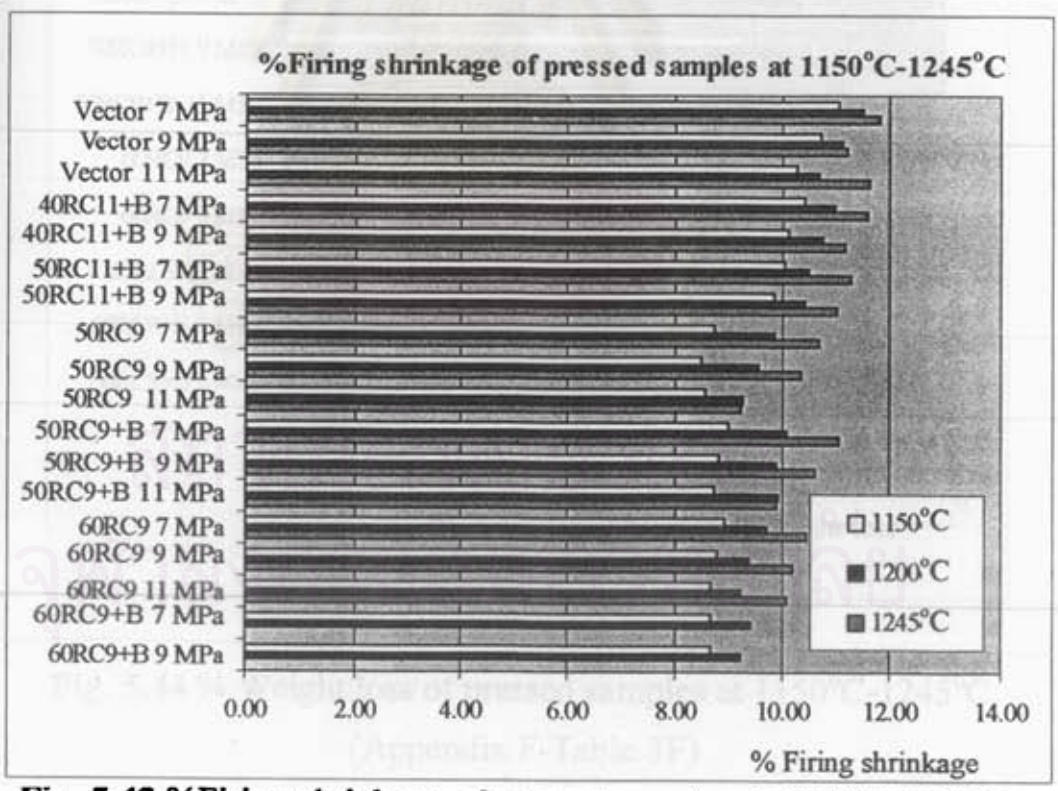

Fig. 5.43 %Firing shrinkage of pressed samples at 1150°C-1245°C.
(Appendix F-Table 3F)

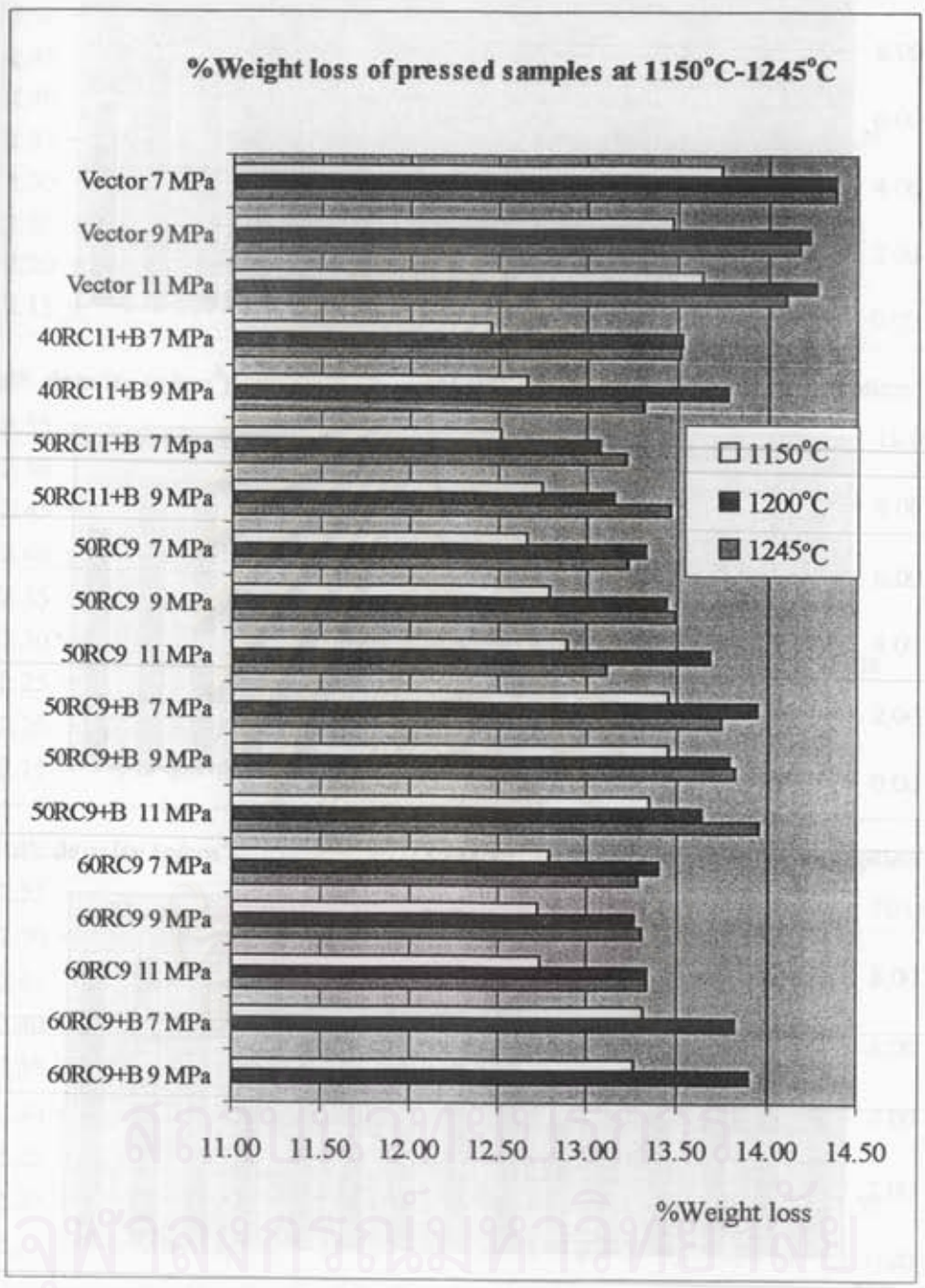

Fig. 5.44 % Weight loss of pressed samples at 1150°C-1245°C.
(Appendix F-Table 3F)

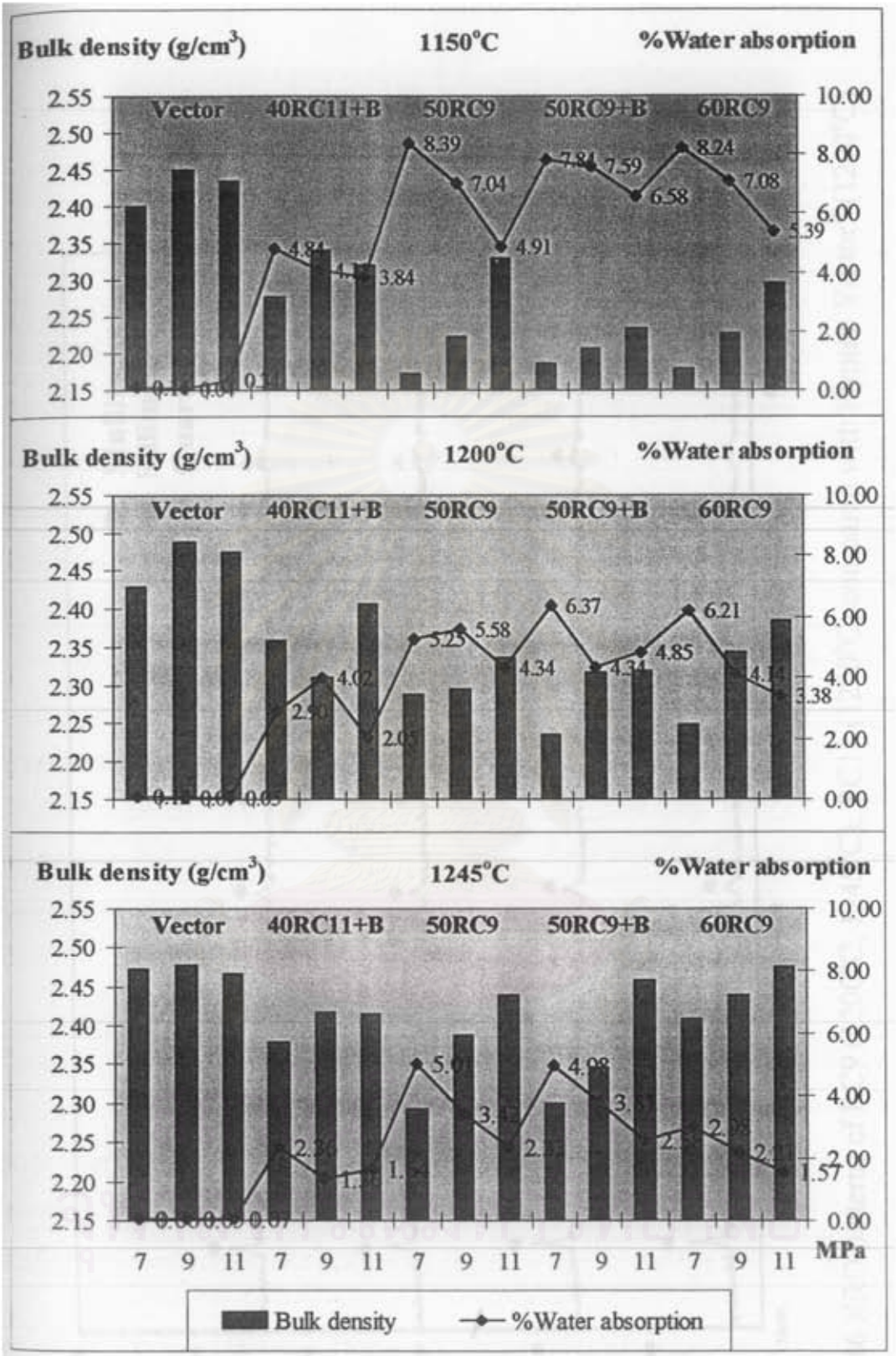

Fig. 5.45 Bulk density and %water absorption of pressed samples at 1150°C-1245°C. (Appendix F-Table 3F)

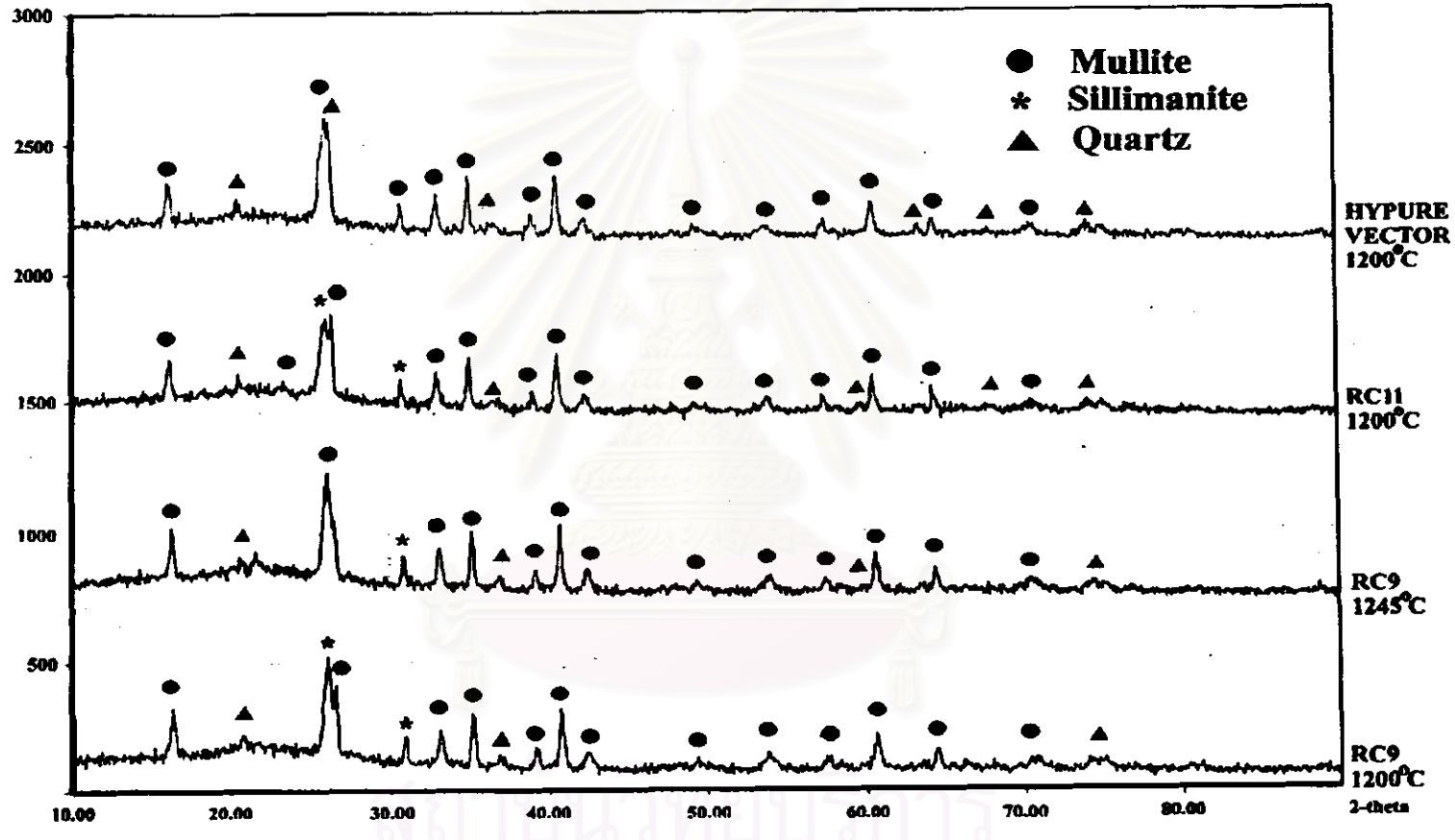

Fig. 5.46 XRD patterns of RC9 (1200°C, 1245°C), RC11 (1200°C) compared with Hypure Vector® (1200°C)